OPTICAL TRAPPING: FORCE MEASUREMENT AND THE INVESTIGATION OF BACTERIAL PHYSIOLOGY

A thesis presented to the faculty of
San Francisco State University
In partial fulfilment of
the Requirements for
the Degree

Master of Science
In
Physics

by

Chensong Zhang

San Francisco, California

August 2017

CERTIFICATION OF APPROVAL

I certify that I have read *OPTICAL TRAPPING: FORCE MEASUREMENT AND THE INVESTIGATION OF BACTERIAL PHYSIOLOGY* by Chensong Zhang and that in my opinion this work meets the criteria for approving a thesis submitted in partial fulfillment of the requirements for the degree: Master of Science in Physics at San Francisco State University.

Zhigang Chen, PhD
Professor of Physics

Huizhong Xu, PhD
Associate Professor of Physics

Roger Bland, PhD
Professor Emeritus of Physics

OPTICAL TRAPPING: FORCE MEASUREMENT AND THE INVESTIGATION OF BACTERIAL PHYSIOLOGY

Chensong Zhang
San Francisco State University
2017

This thesis is concerned with the optical trapping and analysis of biological specimens. The change in momentum of light due to the interaction between light and matter generates force. Optical trapping permits the manipulation of microscopic objects, detection of nanometer displacements, and piconewton forces without any mechanical contact. There are multiple methods to analyze the optical forces exerted on the specimens. Preferable methods are calculating forces through viscous drag force and power spectral density. Trap parameters in the detection of bacterial motility are intractable. Hence, the analysis of the autocorrelation function for the bacterial motion has been purposed and has successfully shown a similar result in bacterial ethanol toxicity in the presence of alcohol. The optical trap is a tightly focused beam and induces damage to the specimen. More significantly, photon-induced damage by optical trapping is dependent on bacterial growth conditions. This thesis strives to use to optical trapping to analyze bacterial damage in a single cell experiment.

I certify that the Abstract is a correct representation of the content of this thesis.

Dr. Zhigang Chen, Chair, Thesis Committee Date

ACKNOWLEDGMENTS

I would like to thank Dr. Zhigang Chen for giving me the opportunity to work and to learn in his lab, and for his support and assistance on all of the projects I have worked on during my time at San Francisco State University. This has been an amazing experience. I would like to thank my committee members, Dr. Roger Bland and Dr. Huizhong Xu. Dr. Bland assisted me with my experimental and computational questions. Dr. Xu was essential for taking our research to a new level. I would like to thank Dr. Weining Man, who got me started down this path and helped me the whole way, and Dr. Joseph Chen and his crew for their support in biology. I would like to thank the postdoctoral fellows that I have had the pleasure to learn from and work with. Dr. Yuxuan Ren was with me through the countless hours of experimental and theoretical work; we accomplished a great deal together. Dr. Rekha Gautam and I spent countless hours on troubleshooting experiments. Dr. Akbar Samadi taught me my very first lessons in experimental optics. Dr. Anna Bezryadina and Dr. Yong Sun also assisted in our research. I would also like to thank all the students I have had the pleasure of working with in the lab, Daniel Gallardo, Drew Bischel, Trevor Kelly, Graham Siggins, Stephen Nenni, Jeff Butler, Josh Lamstein, Eric Dyer and Pepito Alvaro. They were essential for our Optical Society (OSA) Student Chapter at San Francisco State University. I would also like to

thank all the professors in the Physics and Astronomy Department at San Francisco State University, for their hands in my physics education. I would also like to thank my family and Ms. Shujia Guo for their continuous support.

TABLE OF CONTENTS

1 Introduction 1

2 Optical Forces 3

2.1 Rayleigh Regime 8

2.1.1 Scattering Force in the Rayleigh Regime 8

2.1.2 Gradient Force in the Rayleigh Regime 9

2.2 Mie Regime 10

3 Optical Trapping 14

3.1 Construction of Optical Trapping 15

3.1.1 Illumination System 16

3.1.2 Trapping System 17

3.1.3 Control System 20

3.1.4 Detection System 23

3.2 Upgrade 27

4 Force Calibration and Measurement 30

4.1 Calibration Methods 31

4.1.1 Equipartition Theorem Method 31

4.1.2 Power Spectral Density Method 34

4.1.3 Viscous Drag Force Calibration 37

4.2 Experimental Setup 39

5 Chemotaxis in Optical Trapping 42
5.1 Introduction 43
5.2 Experimental setup and method 45
5.3 Experimental results and analysis 48
5.4 Conclusion 51

6 Phototaxis in Optical Trapping 56
6.1 Introduction 57
6.2 Experimental setup and method 59
6.3 Experimental results and analysis 63
6.4 Conclusion 69

7 Conclusion 73

Appendix A Essential Calculations 76
A.1 Force Calculations 76
A.1.1 Rayleigh Regime 76
A.1.2 Mie Regime 81
A.2 Calculations in the Steering System 84
A.2.1 Steering in the Axial Direction 85
A.2.2 Steering in the Transverse Direction 89
A.3 Calculations of Calibration Methods 94
A.3.1 Power Spectral Density Methods 94

A.3.2 Viscous Drag Force Calibration 96

Appendix B Experimental Procedures 100

B.1 Optical Trapping 100

B.1.1 Operation of a Laser 100

B.1.2 Operation of a Microscope 102

B.1.3 Optical Tweezers 104

B.1.4 Shutting Down 105

B.2 Immunocytochemistry Experiment 106

B.2.1 Experimental Procedures 106

B.2.2 Materials Needed 108

B.2.3 Instruments 110

B.3 Colony-Forming Unit Experiment 110

B.3.1 Experimental Procedures 111

B.3.2 Materials Needed 113

B.3.3 Instruments 114

Bibliography 115

LIST OF TABLES

Table Page

6.1 Results of colony-forming unit experiments 68

LIST OF FIGURES

Figure		Page
2.1	Schematic of a trapped particle in a parallel beam	6
2.2	Schematic of a trapped particle in a focused beam	7
2.3	Ray tracing in a particle in the Mie regime	12
3.1	Schematic of an optical trap	16
3.2	Schematic of a quadrant position detector	25
4.1	Schematic of the experimental setup for force measurements	41
5.1	Schematic of the experimental setup for chemotaxis investigation	53
5.2	Results of autocorrelation function	54
5.3	Normalized ACF (ζ) vs. time for different alcohol concentrations	55
6.1	Schematic of optical tweezers combined with dark-field microscopy	70
6.2	Results of image processing	71
6.3	Histograms of characteristic shrinkage time constants τ of trapped *E. coli*	72
A.1	Schematic of Steering in the Axial Direction	85
A.2	Schematic of Steering in the Transverse Direction	89

Chapter 1

Introduction

Light produces forces on matters by a momentum exchange, as demonstrated by Ashkin's optical levitation in 1976. Furthermore, he expanded his ideas and came up with an extraordinary instrument that achieves a three-dimensional confinement, which is so-called "optical trapping"and is often referred to as "optical tweezers". Optical trapping has become an excellent tool to measure force in the range of picoNewtons without mechanical contact. As technology advances, it is widely used to investigate molecular machinery and bacterial physiology. In Chapter 2, optical forces, composed into gradient and scattering forces, are derived in both Rayleigh and Mie regimes which can be measured by an optical trap. Chapter 3 introduces the background and the design of optical traps. Methods and experiments of force calibration and measurement using optical trapping are introduced in Chapter 4. Although

those methods for force measurement are commonly used in investigating bacterial physiology, we purpose a statistical analysis of time series for bacterial motion. As a proof of concept, our methods are verified by measuring the "killing time" of *Escherichia coli* in the presence of alcohol in Chapter 5. Although infrared lasers are highly recommended in trapping biological specimen, a tightly focused beam at the trapping point induces damage at the specimen. Combining dark-field microscopy and optical trapping, a detailed investigation on photon-induced damage by 532 nm on *E. coli* is shown in Chapter 6. Overall, a brief summary is in given Chapter 7.

Chapter 2

Optical Forces

Light can exert forces because photons are elementary particles which carry electromagnetic energy and momentum. They have zero rest mass and exhibit wave-particle duality. In special relativity, the invariant length of the energy-momentum 4−vector is

$$p_0^2 - \vec{p} \cdot \vec{p} = (m_0 c)^2 , \tag{2.1}$$

where $p_0 = \frac{E}{c}$ and m_0 is the particle rest mass. Or, Eq.2.1 becomes

$$E^2 = c^2 p^2 + m_0^2 c^4,$$

by substituting p_0, where p is the magnitude of the momentum vector $\vec{p}$. Because a photon has zero rest mass, the energy and momentum of a photon are related by

$$E = cp. \tag{2.2}$$

In addition, the Planck-Einstein relation states that the energy of a photon, E, is proportional to its frequency, ν:

$$E = h\nu = \frac{hc}{\lambda}, \tag{2.3}$$

where h is the Planck constant. Substituting Eq.2.3 into Eq.2.2, the magnitude of the momentum p of a photon becomes:

where $k = \frac{2\pi}{\lambda}$ is the wave number and $\hbar = \frac{h}{2\pi}$ is the reduced Planck constant. Since $\vec{p}$ is in the propagation direction of a photon, the momentum $\vec{p}$ of a photon is

$$\vec{p} = \hbar\vec{k}, \tag{2.4}$$

where $\vec{k}$ is the wave vector. This is the de Broglie relation. Eqs.2.3 and 2.4 indicate the energy and momentum of a photon only depend on its frequency, ν or its wavelength, λ.

Although photons are massless particles, they do carry momentum and exert forces by scattering, absorption and radiation. According to Newton's Second Law, the surface of an object exerts a force on the photons

in changing their momentum:

$$\vec{F} = \frac{d\vec{p}}{dt}.$$

An equal and opposite reactive force is then applied to the object based on Newton's Third Law, which are called "optical forces"and will be discussed in details later in this chapter.

Considering a dielectric particle in the presence of a tightly focused Gaussian beam (TEM_{00}), the focal point of the beam contains a very strong electric field gradient. The dielectric particle is pulled to the gradient to the region of strongest electric field, which is the center of an optical trap. Thus, the pulling force acting on the particle is known as the gradient force. When a trapped particle tends to displace from the trap center, a net force restores the particle to the trap center because of a larger momentum change from the more intense beam close to the trap center compared to a smaller momentum change from less intense beams further away from the center. The net momentum change causes a restoring force that pulls the particle to the trap center. In addition, the beam also tends to apply a force on particles, known as scattering force, along the direction of beam propagation because of the conservation of momentum. Photons absorbed and/or scattered by the particle also transfer momentum to the particle. As a result, the particle is displaced

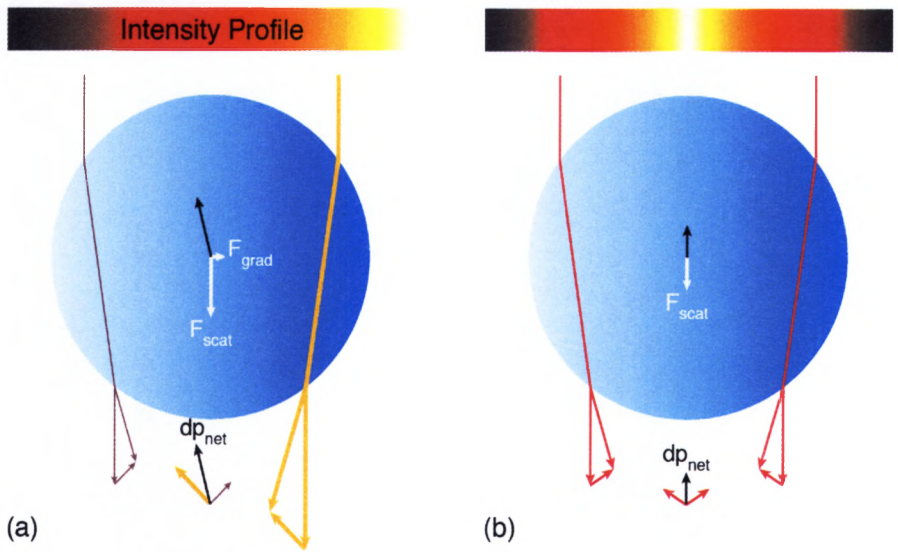

Figure 2.1: Schematic of a trapped particle in a parallel beam. (a) When the particle is located off-center of the beam, with more intense beam (white) close to the trap center, the momentum change is larger compared to the change from less intense beam (brown) further away the center. The net momentum change causes a gradient force that pulls the particle to the most intense region and a scattering force that pushes the particle along the propagation direction.(b) When the particle is located at the beam center, individual rays refract through the particle symmetrically, giving no force in the transverse direction. Overall, the net force in this case is along the axial direction of the trap, which is purely the scattering force.

sightly downstream from the focal point of the beam. Furthermore, the equilibrium trapping point, at which no net force acts on the particle due to the scattering force, is canceled out by the gradient force and is not exactly at the focal point of the beam but slightly downstream of the trap center.

These forces are dependent on refractive indices of the particle and the

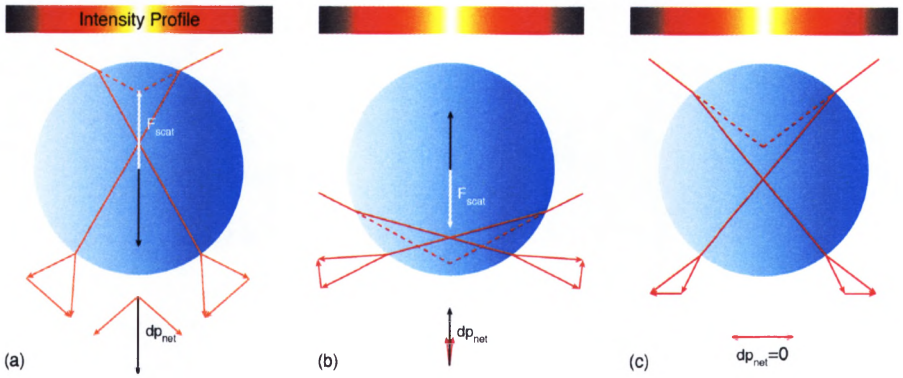

Figure 2.2: Schematic of a trapped particle in a focused beam. (a) & (b) When the particle is located at the center of the beam but away from the equilibrium trapping point, the net momentum change causes an axial gradient force that pulls the particle towards the most intense region. (c) When the particle is located at the equilibrium trapping point, individual rays refract through the particle symmetrically, resulting no net momentum change in transverse and axial directions of the trap. Thus, the axial gradient force in this case cancels out the scattering force of the beam. The cancellation is what causes a particle to be stably trapped at the equilibrium trapping point, slightly downstream of the trap center.

surrounding medium, the geometry of the particle, the wavelength, polarization, mode structure, and the power of the beam. In order to calculate the forces acting on the particle, depending on the particle size, optical forces are analyzed in the Rayleigh regime, in which the trapped particle dimension is within an order of magnitude of the trapping beam wavelength, and the Mie regime, in which the particle dimension is significantly greater than the wavelength of the trapping beam.

2.1 Rayleigh Regime

For a perfect spherical dielectric particle with radius a trapped in an optical trap, the dimension of the object is within an order of magnitude of the trapping beam wavelength. Hence, the forces are calculated by involving either the time dependent or time-harmonic form of Maxwell equations using appropriate boundary conditions. In addition, particles in this regime can be treated as electric dipoles in an electric field because light momentum cannot be traced.

2.1.1 Scattering Force in the Rayleigh Regime

Light can exert radiation pressure on any object it encounters and that resulting optical force can used to manipulate particles. Light always pushes a particle along its direction of propagation. The scattering force, pointing in the direction of the incident light, is given as [1]:

$$F_{\text{scat}} = \frac{128\pi^5 a^6}{3c\lambda^4} \left(\frac{m^2 - 1}{m^2 + 2} \right)^2 n_2 I\left(\vec{r}\right),$$

where c is the speed of light, a is the particle radius, λ is the wavelength of the trapping beam, $I\left(\vec{r}\right)$ is the intensity of the beam, n_2 is the refractive index of the surrounding medium, and m is the ratio of refractive indices of the trapped particle and the background medium. A stable optical

trapping requires the balance of the gradient force and the scattering force at the equilibrium trapping point.

2.1.2 Gradient Force in the Rayleigh Regime

The gradient force mainly comes from strong electric field gradient. With a tightly focusing laser beam, if the refractive index of a particle is greater than that of the background medium, the gradient force pushes the particle in the direction of the gradient of the electric field, so that the particle tends to enter in the region of the highest field strength. In other words, the gradient force is a restoring force that pulls the particle into the center of the highest light intensity region. Arising from the gradient of the Gaussian intensity profile and pointing in the lateral plane towards the center of the highest intensity, the gradient force is given as [1]:

$$F_{\text{grad}} = \frac{2\pi a^3}{c}\left(\frac{m^2-1}{m^2+2}\right) n_2 \nabla I\left(\vec{r}\right),$$

Note that in case of $m > 1$ where the refractive index of the particle is greater that the background medium, the gradient force is positive and attractive. Vice verse when $m < 1$. The gradient force transverse components $\vec{F}_{\text{grad},x}\left(\vec{r}\right)$ and $\vec{F}_{\text{grad},y}\left(\vec{r}\right)$ reach their maximum at $\left(\pm\frac{w_0}{2}, 0, 0\right)$

and $\left(0, \pm\frac{w_0}{2}, 0\right)$ and the axial component $\vec{F}_{\text{grad},z}(\vec{r})$ reach its maximum at $\left(0, 0, \pm\frac{kw_0^2}{2\sqrt{3}}\right)$, where w_0 is the beam waist and k is the wavenumber. The equilibrium trapping point is thus located at slightly downstream of the trap center as mentioned above.

2.2 Mie Regime

Consider a perfect spherical dielectric particle with radius a trapped in an optical trap. The dimension of the particle is much greater than the wavelength of the trapping beam, so the trapping phenomenon can be explained sufficiently using ray optics. As shown in Fig.2.3, individual rays emitted from the laser are refracted as they enter and exit the particle. Due to the conservation of momentum, the bending of light indicates that light momentum is changed and transferred to the particle. Thus, the particle gains an equal but opposite momentum change, that results in forces acting on the particle. For a single ray, forces can be shown to be [2]:

$$f_{\text{scat}} = \frac{n_2 P}{c}\left(1 + R\cos 2\theta - \frac{T^2\left(\cos(2\theta - 2\theta_{\text{refr}}) + R\cos 2\theta\right)}{1 + R^2 + 2R\cos 2\theta_{\text{refr}}}\right),$$

and

$$f_{\text{grad}} = \frac{n_2 P}{c}\left(R\sin 2\theta - \frac{T^2\left(\sin(2\theta - 2\theta_{\text{refr}}) + R\sin 2\theta\right)}{1 + R^2 + 2R\cos 2\theta_{\text{refr}}}\right),$$

where c is the speed of light, P is the power of the trapping beam, n_2 is the refractive index of the surrounding medium, R and T are the Fresnel reflection and transmission coefficients of the surface at θ, and θ and θ_{refr} are the angles of incidence and refraction.

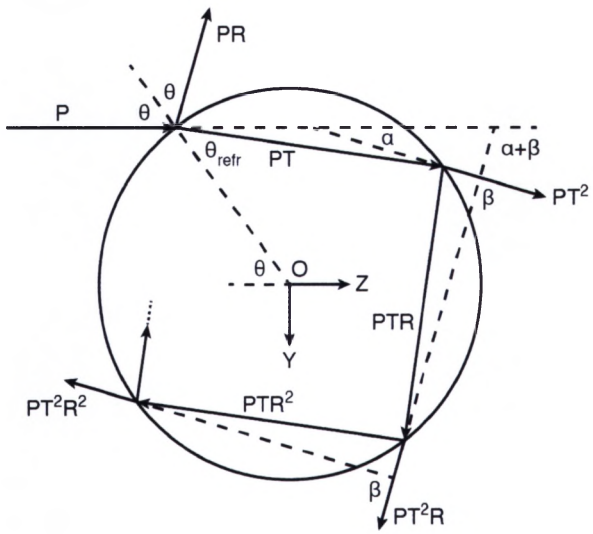

Figure 2.3: Ray tracing in a particle in the Mie regime. Assume a ray of power P hits the particle at an angle θ where it partially reflects and refracts, giving rise to a series of scattered rays of power PR, PT^2, PT^2R, ..., PT^2R^n, ... The angles relative to the incident ray are $\pi + 2\theta$, α, $\alpha + \beta$, ..., $\alpha + n\beta$, ..., where $\alpha = 2\theta - 2\theta_{\text{refr}}$ and $\beta = \pi - 2\theta_{\text{refr}}$.

Hence, the overall forces acting on the trapped particle are

$$\begin{aligned} F_{\text{scat}} &= \int_0^{\frac{\pi}{2}} d\theta \int_0^{2\pi} d\phi f_{\text{scat}}, \\ &= \int_0^{\frac{\pi}{2}} d\theta \int_0^{2\pi} d\phi \frac{n_2 P}{c} \left(1 + R\cos 2\theta - \frac{T^2\left(\cos(2\theta - 2\theta_{\text{refr}}) + R\cos 2\theta\right)}{1 + R^2 + 2R\cos 2\theta_{\text{refr}}} \right), \end{aligned}$$

and

$$\begin{aligned} F_{\text{grad}} &= \int_0^{\frac{\pi}{2}} d\theta \int_0^{2\pi} d\phi f_{\text{grad}}, \\ &= \int_0^{\frac{\pi}{2}} d\theta \int_0^{2\pi} d\phi \frac{n_2 P}{c} \left(R\sin 2\theta - \frac{T^2\left(\sin(2\theta - 2\theta_{\text{refr}}) + R\sin 2\theta\right)}{1 + R^2 + 2R\cos 2\theta_{\text{refr}}} \right). \end{aligned}$$

A detailed calculation is given in Appendix A.1.

Forces generated on a trapped particle consist of scattering and gradient forces due to the interaction of the particle with the beam. When the particle is displaced from the trap center, the gradient force acts as a spring force, that is proportional to the displacement from the center. In practice, without applying any external force, the particle motion is Brownian. Whenever the particle tends to leave the center, the gradient force pulls it back to the center. Optical trapping has many applications in many different fields, especially in physics, biology and biochemistry. For instance, it is capable of measuring small forces and weak interaction in biological systems, such as the interaction of molecular motors with

microtubules, the elasticity of DNA molecules, the compliance of bacterial flagella, etc. However, because a tightly focused trapping beam usually is applied directly to trapped particles and photon-induced damage is less well understood, optical trapping has to be carefully considered prior to and during the usage.

Chapter 3

Optical Trapping

Optical trapping, often referrred to as "optical tweezers", uses light to manipulate microscopic dielectric objects ranging in size from 10 nm to over 100 µm, neutral atoms (0.1 nm in diameter) by utilizing a resonant laser beam and a magnetic gradient trap which is referred to as a magneto-optical trap, and to measure nanometer displacements and piconewton forces. Due to optical forces generated on a dielectric particle, which has been discussed in detail in Chapter 2, and the detection of optical scattering and gradient forces on micron sized particles [3], the first demonstration of modern optical trapping has shown the capability to hold microscopic particles stable in three dimensions [1]. Nowadays, optical trapping has been an excellent tool to study different biological phenomena, for instance, confinement and organization of cells by creating an intensity pattern over the sample area [4], cell motility by tracking

of bacterial motion, altering of cell membranes to investigate electromechanical properties across membranes [5], measurement of viscoelastic properties of biopolymers [6], measurement of small forces generated by molecular-scale biological motors [7], etc. Scientists like Carlos Bustamante, James Spudich, and Steven Block were pioneers in applying optical trapping to characterize molecular motors which are ubiquitous and responsible for locomotion and intracellular mechanical action. Because optical trapping is so complicated and requires a knowledge of microscopy, optics, and laser techniques, this chapter will focus on the design of such an instrument in a great detail.

3.1 Construction of Optical Trapping

Optical traps are very expensive, custom-built instruments, that typically start with a commercial inverted optical microscope. A good laser source is mandatory and has to be coupled into the microscope by a dichroic mirror to achieve a three-dimensional confinement with the help of an objective lens. High-power infrared laser beams are often used to achieve high trapping stiffness with minimal photodamage to biological samples [8]. To manipulate and detect nanometer displacements on a microscopic particle, advanced control and detection systems are required.

We will start the discussions about illumination, trapping, control and detection systems, the four essential components that are made up a simple optical trap.

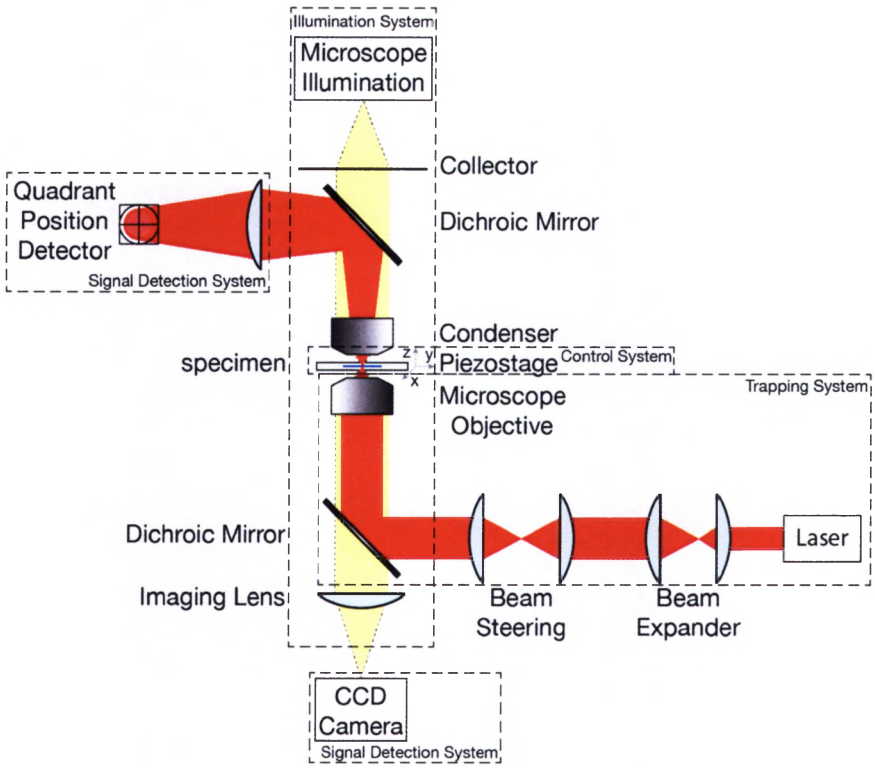

Figure 3.1: Schematic of an optical trap.

3.1.1 Illumination System

A simple optical microscope, consisting of an objective lens, a condenser, and an illumination source, is capable of creating a stable trap and mon-

itoring specimen simultaneously. In general, an inverted microscope is recommended. An objective lens provides tight focusing of the beam to create the axial gradient of a trap. As a part of the illumination system, a condenser also plays a role in the detection system, which will be covered in latter section. An optical microscope could be assembled from scratch, which is good for a small budget and has more freedom to be modified and upgraded. However, it requires more effort to achieve Köhler illumination, that provides an even illumination of the sample and an invisible image of the illumination source at the imaging plane. Alternatively, a commercial modern optical microscope, which requires a large budget, is more convenient because of built-in Köhler illumination. However, modification and upgrade are limited by the design of the microscope.

3.1.2 Trapping System

In general, the trapping systems consist of a laser source, pairs of lenses for beam expansion and steering purposes, and an objective lens.

Laser

In principle, any type of laser can be considered as a trapping source. However, a laser with near-infrared and infrared wavelength is highly rec-

ommended to work with biological samples because of a low absorption coefficient at such wavelengths [8]. Decreasing the absorption may minimize damage to the specimens. In fact, whichever wavelengths of laser sources are selected, the intense laser beam at the trap center somehow causes photon induced damage ("photodamage") on trapped particles. For instance, visible to infrared light can excite oxygen molecules in aqueous solutions to generate free radicals, which are highly chemically reactive and induce damage to the specimens. In Chapter 6, an investigation on the correlation between cell growth conditions and the resistance of photodamage is reported. A dichroic mirror is placed after the condenser, which reflects the light coming from the trap and permits the illumination light to go through. Most optical traps apply conventional TEM_{00} Gaussian beams. However, a number of other types of beams have been used to trap particles as well, such as high order Hermite-Gaussian beams (HG), Laguerre-Gaussian (LG) and Bessel beams. The instrument based on LG beams have the unique capability of possessing an orbital angular momentum that can rotate particles without external mechanical or electrical steering of the beam [9] [10]. Both zero and higher order Bessel beams are able to trap and rotate multiple particles that are millimeters apart and even around obstacles [11].

Beam Expansion and Steering

Beam expansion and steering consist of several convex lenses. To avoid spherical aberration, a set of plano-convex lenses is preferred. A pair of convex lenses expand and collimate the laser beam. More importantly, expanding the beam emitted from a laser source to fill the entrance pupil of an objective lens results in a tighter, diffraction-limited spot at the specimen plane [8]. Similar to beam expansion, two pairs of convex steering lenses are preferred to achieve a full steering of the trap center at the specimen plane. Calculations about how steering lenses affect the trap center at the specimen plane are given in Appendix A.2.

Objective Lens

The most important consideration in a optical trap design is the choice of an objective lens that is critical to determine overall efficiency of the trap. Both the numerical aperture (NA) and the transmittance of an objective lens are primary factors that affect trap stiffness and beam input power. The three-dimensional confinement of a trap requires the counterbalance of the axial gradient force to the scattering force, which the gradient force is strongly dependent upon the NA. In general, an microscope objective lens with an NA between 1.2 and 1.4 is selected [12]. In addition, the working distance and the immersion medium of the

objective lens limit the depth to which particles can be trapped. Note that the refractive index mismatch between the immersion medium and the aqueous trapping medium causes spherical aberration, that degrades trapping performance with increasing focal depth. The maximum axial range from cover slides into the trapping chamber is 5 to 20 µm [13]. The guideline of choosing an objective lens for optical trapping is given in Ref. [9] [14] [15] and [16].

3.1.3 Control System

The importance of a precise calibrated dynamic trap position control not only allows particles to be manipulated in the trapping chamber, but also permits the forces acting on particles to be varied in real time, which has been applied to generate both force and position clamp measurement conditions [17] [18]. Trap position control by Acousto-optic deflectors (AODs), galvanometer-driven mirrors, or spatial light modulators (SLMs) permits beam steering at the specimen and generates multiple traps by sharing a single laser beam or a line trap. Note that this control method only is valid when the trap position is scanned at a rate faster than the relaxation time of the Brownian motion of a trapped particle [19]. As a comparison, a piezoelectric (PZ) stage, which has great position sensitivity, is commonly applied in optical trapping to control

the sample position relative to the trap center.

Spatial Light Modulator

An SLM is a device that spatially and temporarily modulates amplitude and phase of a beam of light. It is commonly used in overhead projection, holographic data storage, holographic display technology, optical computing, etc. In general, an optical trap uses one laser source to create one or two traps at the specimen plane by splitting the laser beam into two orthogonally polarized beams. Alternatively, two independent laser sources are applied to generate two traps at the specimen plane, which is often referred to as "dual trap". Applying SLMs, two or more traps can be realized either by time-sharing a single laser beam among several optical tweezers [9] [20] or by diffractively splitting the beam into multiple traps. Such an instrument implemented with an SLM often refers to a holographic optical trap that are capable of moving objects in three dimensions [21]. Advanced holographic optical traps with arbitrary spatial profiles find applications from micromanipulation to ultracold atoms [22]. In our lab, a tug-of-war trap generated an SLM is reported the capability to study the strength of cell clusters in biofilm formation.

Piezoelectric Stage

A PZ stage is a device that provides a stable, linear, reproducible, ultra-fine positioning in three dimensions. For the latest generation of commercial PZ stages with capacitive feedback, the positional uncertainty is 1 nm. A PZ stage controls the specimen position in three-dimensions inside the trapping chamber. Improving accuracy of the stage makes position measurement and force calibration faster, more reproducible and more precise [23]. Incorporating capacitive position sensing into a force feedback loop [24] [25] [26] [27], the stage allows constant-force measurement of an arbitrary displacement. The precise position control in the axial dimension allows characterization of the longitudinal properties of optical trapping, such as the radiation pressure measurement. However, communication with the stage controller, which the typical maximum rate is around 50 Hz [28], can be slower compared with the method of controlling trap position. In addition, PZ stages are expensive. Nowadays, a three dimensional stage with capacitive feedback plus a digital controller costs more than $\$20,000$.

3.1.4 Detection System

Most optical trapping is built up on optical microscopy. There exist several ways of measuring the position of a trapped particle. Visualization of the specimen is usually accomplished through Köhler illumination via a light source, which is considered as a common detection method, especially in the presence of multiple traps. However, for a single beam trap, the most common method is back-focal-plane (BFP) interferometry, which analyzes the beam exiting the trap and collected by the condenser on a quadrant photodiode detector (QPD).

Video and Frame Analysis

Videos of trapped particles are easily obtained with a charge-coupled device (CCD) or complementary metal-oxide-semiconductor (CMOS) camera attached to the microscope. A tracking program measures transverse displacements of trapped particles by image processing techniques in order to locate the center of mass of a particle with subpixel resolution. In each frame, a low pass filter is applied to reduce the camera noise. An additional shape detection nonlinear filter accentuates the contours of the particles. Then, the frame is converted to a binary image using a threshold value either manually or automatically selected and the particles on each frame are dilated to ensure that all the contours define closed

shapes and holes are filled. After the previous dilation process, small particles such as dust or camera noise are removed from frames before calculating the centroid of each particle. This process can be done from a video recording but also in real-time by automatically processing each new frame registered by the camera. This method strongly depends on the illumination, particle defocus and particle size. The image processing parameters can be adjusted depending on experimental conditions to optimize the tracking efficiency. In general, video and frame detection is less accurate than back-focal-plane interferometry, but it has capabilities of imaging and tracking particles in multiple traps simultaneously.

Back-Focal-Plane Interferometry

The beam, exiting the trap and collected by a condenser, contains the light scattered by the sample and that does not interact with the sample. As a result, an interference pattern is formed downstream of the condenser. A dichroic mirror is placed after the condenser that reflects the beam coming from the trap and permits the illumination light go through. At the back-focal-plane (BFP) of the condenser, the interference pattern is projected onto a position sensitive detector by a convex lens. Then, the signal from the detector is analyzed to obtain relative displacements of a trapped particle. To obtain a good signal at the detector

by collecting enough photons, a condenser with high NA is preferred. Choices of a position sensitive detector are numerous, for instance, a lateral position detector, a quadrant photodiode detector (QPD), etc. Here, we will briefly introduce how a QPD works and collects data in optical trapping.

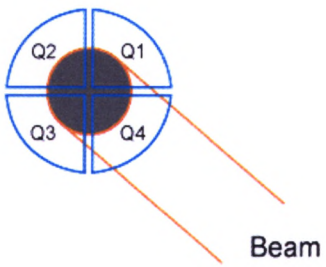

Figure 3.2: Schematic of a quadrant position detector. A segmented-quadrant position sensitive detector with fast response and extraordinary resolution from Thorlabs Inc. (Model No. $PDQ80A$) is used in our lab. A QPD consists of four identically distinct quadrant-shaped photodiodes that are separated by a roughly 0.1 mm gap and together form a circular detection area which are capable of measuring the position of an incident beam in two dimensions.

When the beam is incident on the sensor, light is converted to four currents by the four sectors (denoted as Q_1, Q_2, Q_3 and Q_4 as shown in Fig.3.2). The different signals of the four currents then are determined using an appropriate analog-to-digital converter. The normalized coordinates (X, Y) for the beam location are:

$$X = \frac{(Q_2 + Q_3) - (Q_1 + Q_4)}{Q_1 + Q_2 + Q_3 + Q_4},$$

and

$$Y = \frac{(Q_1 + Q_2) - (Q_3 + Q_4)}{Q_1 + Q_2 + Q_3 + Q_4},$$

where the summation of all four signals for normalization purposes. The summation of the four signals is also treated as the signal in the $Z-$direction and proportional to the beam intensity. If a symmetrical beam is centered on the sensor, four identical currents are generated which results in null difference signals. Hence, the normalized coordinates is $(X, Y) = (0, 0)$ which indicates nothing is in the trap. The four currents change if the beam moves off the center, resulting in different signals as the motion of the trapped particle shifts the beam at the detector. A lateral sensor might be considered if the incident beam is not Gaussian.

For more accurate calibration of the trap stiffness f_c and the drag coefficient γ on any trapping system, which the frequency of the particle motion usually goes up to several kHz, this method does require a detector with bandwidth at least 10 to 100 kHz. Although a high-speed camera can operate at frequencies of 1 to 2 kHz [29], a photodiode position detector with large bandwidth provides higher spatial resolution and is highly recommended when implemented in back-focal-plane interferometry. However, the disadvantage is the lack of tracking and analyzing motions of multiple trapped particles.

3.2 Upgrade

As mentioned, extensive modifications may be considered and introduced into an optical trap system. An amplifier can be introduced into the detection system, which increases signal-to-noise ratio and amplifies the signal of a trapped particle. An optical isolator is good to protect a laser source from back reflection that may occur after the isolator by only permitting light to travel in one direction. Back reflection can damage a laser source orcause it to mode change, amplitude modulate, or frequency shift. In high-power applications, back reflection can cause instabilities and power spikes. More importantly, to simultaneously manipulate and image samples that exhibit fluorescence, optical trapping can be built on a fluorescence microscope [30] [20]. Alternatively, fluorescence module can be introduced. Such instruments are particularly useful when studying biological molecules that have been fluorescence-labelled or in applications in which fluorescence is used to track and visualize objects that are to be trapped, for instance, in the study of molecular motors and the physical properties of DNA [20] [23] [26]. In both areas, a biological specimen is usually attached to a micron-sized fluorescent sphere that is then trapped. By attaching a single molecular motor (such as kinesin, myosin, RNA polymerase etc.) to such a sphere, we have been able to probe motor properties such as the step size that

the motor takes and the measurement of force that the motor produces. Similarly, by attaching the spheres to the ends of single pieces of DNA, the elasticity of the DNA is measured, as well as the forces under which the DNA breaks or undergoes a phase transition.

Optical trapping with sophisticated devices under computer control is capable of manipulation and detection of sub-nanometer displacements for sub-micron dielectric particles [31]. However, to achieve the greatest sensitivity, stability, and signal-to-noise ratio of such an instrument, experimental environments have to be carefully controlled. Temperature changes, mechanical vibrations, acoustic noise and air convection can affect the instrument performance. Thermal fluctuations can lead to slow, large-scale drifts. A 1 K temperature increment easily leads to micrometers of drifting over a long period of experiment. Acoustic noise can shake optical components that couple the laser into the objective, the objective itself and the detection system that lies downstream of the objective. Mechanical vibrations arise from heavy building equipment, compressors or pumps operating nearby, passing traffic on a roadway, etc. Low-frequency mechanical vibrations can be also induced by air currents which can causes various optical perturbations such as light scattering by airborne dust particles. Hence, reducing ambient noise sources is commensurate with precisely controlled measurements. Isolating the in-

strument from noisy power supplies, heat sources, computers, etc. can reduce thermal effects, acoustical and mechanical vibrations. Shortening the measurement time can avoid thermal drift. A passive air table offers a mechanical isolation at frequencies above 1 to 2 Hz. Mechanically rigid optical mounts can reduce resonance and vibration by placing them as close to the optical table as feasible in order to achieve acoustic noise isolation. Enclosing all the free-space along the beam path can improve both mechanical and optical stability of the instrument by reducing ambient air currents. In short, optical traps are very sensitive instruments and are capable of manipulation of micron-sized objects and measuring displacements and forces with high precision and accuracy. For this reason, they are often used to manipulate and study single molecules by interacting with a microsphere that has been attached to that molecule. DNA, proteins [25] [27] [32] and enzymes that interact with it are commonly studied in this way. Researchers have also worked to convert optical tweezers from large complex instruments to smaller simpler ones for use by those with smaller research budgets [33] [34].

Chapter 4

Force Calibration and Measurement

Before measuring forces, the precise calibration of the correlation between a force acting on a particle and displacements between the center of the particle and its trapped equilibrium position must be done. If a trapped particle is displaced not far away from the equilibrium position, the force applied to the particle is linear with respect to the displacement. Hence, a particle trapped optically with small displacements from the equilibrium position can be treated as a mass on a spring system, which follows Hooke's law.

$$\vec{F} = -\kappa \vec{x},$$

where κ is the trap stiffness (a spring-like constant) and $\vec{x}$ is the displacement from the trap center. While a trapped particle is stable inside

a trap, the particle has Brownian motion due to thermal fluctuations. Regardless of any additional external force driving the particle, the trap stiffness is determined. Furthermore, forces acting on the particle can be extrapolated by measuring the displacement of the particle motion inside the trap.

4.1 Calibration Methods

As mentioned, calibration of an optical trap is critical and necessary for all optical trapping experiments. In case where a trapped particle is only driven by thermal fluctuations inside a trap, the Equipartition theorem method offers a relatively fast estimation of trap parameters but is inaccurate compared to power spectral density (PSD) method. If an additional external force is applied to the particle (i.e. moving the trap position and/or the specimen stage), calibration by using drag forces is sufficient to determine the trap stiffness. We will discuss those three methods briefly.

4.1.1 Equipartition Theorem Method

An optically trapped particle moves randomly inside a trap if only thermal force is acting on it. Hence, the shape of the trapping potential can

be determined then applied to the calibration of the trap. Furthermore, the Boltzmann distribution is used to describe any continuous trapping potential that is associated with thermal fluctuations. At equilibrium, the probability density function (PDF), $\rho(x, y)$, of the Boltzmann distribution for optically trapped particle displacements is:

$$\rho(x, y) = C \exp\left(-\frac{U(x)}{k_B T}\right),$$

where k_B is the Boltzmann constant, T is the absolute temperature, $U(x)$ is the potential energy, and C is a normalization constant. According to statistical mechanics, for each degree of freedom in thermal fluctuations, the equipartition method for a trapped particle fluctuating in a harmonic potential gives

$$\frac{1}{2} k_B T = \frac{1}{2} \kappa_x \left\langle x^2 \right\rangle,$$

where κ_x is the trap stiffness and $\langle x^2 \rangle$ is the variance of the displacements. Hence, the trap stiffness is determined by measuring the temperature and the variance in displacements of an optically trapped particle. Furthermore, the PDF of Boltzmann distribution becomes a simple Gaussian PDF parametrized by κ_x and κ_y:

$$\begin{aligned}\rho(x,y) &= C\exp\left(-\frac{U(x,y)}{k_BT}\right), \\ &= C\exp\left(-\frac{\kappa_x}{2k_BT}(x-x_0)^2\right)\exp\left(-\frac{\kappa_y}{2k_BT}(y-y_0)^2\right),\end{aligned}$$

where κ_x and κ_y are the trap stiffness in the corresponding axes, and (x_0, y_0) is the equilibrium position of a trap. Because the viscous drag of the particle does not affect the calibration done in this method, the stiffness can be measured even though the shape of the particle, the trapping depth and the viscosity of the medium are unknown. This simple method, however, is inaccurate compared to the PSD method because the displacement variance is biased. Any noise and drift in displacements affect the determination of the trap stiffness. For instance, displacement signals after a low-pass filter have a smaller variance which results an apparently increase in trap stiffness measurement. In contrast, signals of the particle displaced far from the equilibrium position have a larger variance which yields a softer trap stiffness than the real one.

When a trapped particle is displaced far away from the equilibrium position, Hooke's law fails because the trapping potential is no longer harmonic. However, the histogram of displacements of a trapped particle can be used in the shape construction of anharmonic trapping potential

by solving for $U(x, y)$. As a result, forces acting on the particle in the outer part of the trap can be extrapolated. This approach is only valid with low-noise and low-drift displacement signals because displacement signals with high relative uncertainties contain the anharmonic potential information [35]; however, the number of those signal are few. Although the bandwidth requirements for this method and the PSD method are identical, the PSD method is more accurate for the determination of trap stiffness than the Equipartition theorem method because the displacement variance does not provide additional information about the trap or the detection system [12]. Note that whenever displacements of a trapped particle are detected by a QPD, a conversion factor from V to nm or µm needs to be calculated as well.

4.1.2 Power Spectral Density Method

The power spectral density (PSD) analysis for the displacements of a trapped particle is always considered to be the most reliable method to calibrate optical trapping. Note that the frequencies of the particle motion is related to the trap stiffness. For instance, as the trap stiffness increases, the high frequency components start to dominate the motion of the particle. Under certain conditions, the shape of the PSD for a trapped particle is known, which makes it possible to measure the

trap stiffness by curve fitting on experimental data. Without appling any external forces by physically moving a PZ stage or the trapping position, assume that a particle is trapped at its equilibrium position. The particle motion is governed by the Langevin equation:

$$m\frac{d^2\overrightarrow{x}}{dt^2}+\gamma\frac{d\overrightarrow{x}}{dt}+\kappa\overrightarrow{x}=\overrightarrow{F}_{\text{ext}}(t),$$

where $m\frac{d^2\overrightarrow{x}}{dt^2}$ is the inertia, $\gamma\frac{d\overrightarrow{x}}{dt}$ is the drag force and $\kappa\overrightarrow{x}$ is the trap force. At equilibrium, the trapped particle is moving randomly due to thermal fluctuations, so the only external force acting on the particle is the thermal force. The size of the particle and the fact that it is in aqueous environment makes the particle highly overdamped [36]. Hence, the inertia term can be dropped:

$$\overrightarrow{F}_{\text{ext}}(t)=\gamma\frac{d\overrightarrow{x}}{dt}+\kappa\overrightarrow{x}. \tag{4.1}$$

Then, the PSD for an optically trapped particle that is experiencing Brownian motion is

$$S_{xx}(f)=|X(f)|^2=\frac{k_BT}{\gamma\pi^2(f^2+f_c^2)}.$$

where $f_c\equiv\frac{\kappa}{2\pi\gamma}$ is defined as the corner frequency and a detailed calculation is given in Appendix A.3.1. For low frequencies, $f<f_c$, the PSD

is approximately a constant denoted as S_0:

$$S_{xx}\left(f_{\text{low}}\right) \approx \frac{k_B T}{\gamma \pi^2 f_c^2} \equiv S_0.$$

In high frequency region, $f > f_c$, the density function is inversely proportional to the frequency squared:

$$S_{xx}\left(f_{\text{high}}\right) \approx \frac{k_B T}{\gamma \pi^2 f^2}.$$

With the values of S_0 and f_c acquired from the measurement of the particle inside a trap, the trap stiffness κ and the drag coefficient γ are determined as:

$$\kappa = 2\pi\gamma f_c = \frac{2k_B T}{\pi S_0 f_c},$$

and

$$\gamma = \frac{\kappa}{2\pi f_c} = \frac{k_B T}{\pi^2 S_0 f_c^2},$$

respectively. Note that the drag coefficient $\gamma = 6\pi\eta a$ in Stokes' law is only valid for ideal conditions, for instance the trapped particle is a perfect sphere which is not satisfied in general. As mentioned, for more accurate calibration of the trap stiffness f_c and the drag coefficient γ on

any trapping system, a silicon-based photodiode detector is highly recommended due to larger bandwidth and higher spatial resolution when implemented in back-focal-plane interferometry compared to a camera.

4.1.3 Viscous Drag Force Calibration

Viscous dray force calibration is the most direct method to determine trap stiffness. By moving the stage in a certain pattern, a viscous drag force on a trapped particle can be extrapolated by measuring displacements from the equilibrium position. Because the drag force is generated from the hydrodynamics of a trapped particle, the drag coefficient is known. The force on a sphere with radius a in a viscous medium with viscosity η is described as Stokes' Law:

$$F_{\text{vis}} = 6\pi\eta a v = \gamma v,$$

where v is the velocity of the medium, and γ is the viscous drag coefficient. As mentioned, $\gamma = 6\pi\eta a$ is only valid for idealized conditions that are not always satisfied. A drag force can be also known if the velocity of the medium is given. By measuring displacements of the particle from the equilibrium position aeq:Overdamped Thermal Forcet different forces, such as at different speeds of the medium, the trap stiffness

is determined. Assume that a PZ stage moves following a cosine wave $x(t) = x_0 \cos \omega t$ with frequency f and amplitude x_0, the drag force acting on a trapped particle is

$$F(t) = -\kappa x(t) = -\frac{\kappa x_0}{\sqrt{1 + \left(\frac{f_c}{f}\right)^2}} \sin\left(2\pi f t + \arctan\frac{f_c}{f}\right).$$

A detailed calculation is given in Appendix A.3.2. The advantage of moving the stage using a sine instead of a triangular function is that piezo electronics after a low-pass filter does not modify the shape of the signal sent to the microchamber with amplitude decreasing [35]. To determine accurate values of the amplitude x_0 and the frequency f, an oscilloscope connected to the PZ stage is highly recommended to measure the exiting signal. The bandwidth requirements of the detection system in this method are flexible because the measurement are slow compared with the thermal fluctuations of the particle. However, the maximum frequency f when the stage moves following a triangular function is restricted [35].

4.2 Experimental Setup

Our optical tweezers system is based on an inverted microscope (Axio Observer D1-Zeiss) which is schematically shown in Fig.4.1. A continuous wave laser beam with TEM_{00} transverse mode is expanded by L_1 and L_2 lenses and steered by L_3 and L_4 before it is transmitted into the microscope through the side port. The expanded beam is coupled into the optical pathway of the microscope by a dichroic mirror after which it is tightly focused into the sample chamber using an oil immersion objective lens ($100X$ Zeiss Objective EC Plan-Neofluar) with Numerical Aperture (NA) of 1.3. The sample chamber can be an open-top glass bottom dish (MatTek) or a closed chamber assembled of a plain microscope slide and a cover slide glued by a double-sided tape mounted on a piezoelectric stage (PI NanoXYZ Piezo Stage), providing positional control of the trap inside the chamber with nanometer resolution. The forward scattered light from the trapped particle as well as the direct (un-scattered) light is collected by a condenser lens ($NA = 1.2$). The collected light is reflected off the optical pathway of the microscope by another dichroic mirror and then focused on a QPD situated at the plane conjugate to the BFP of the condenser. Optionally, QPD signals can be amplified by low-noise preamplifiers (Stanford Research Systems) before being transferred to the computer via an Analog-to-Digital (A/D) card

(National Instruments). The QPD positional signals are acquired at a sampling rate of 10 kHz, using a custom-made LabVIEW program [37]. In addition, the trapped particle is monitored with a CCD camera. To avoid hydrodynamic effects of the chamber wall [12], the trap is kept about 10 µm away from the bottom of the dish. In order to exclude artifacts that might be caused by photodamage and heating [38] [14] [39], in addition to implementing other optimization techniques [40], the trapping laser power is kept at no more than 40 mW at the specimen plane.

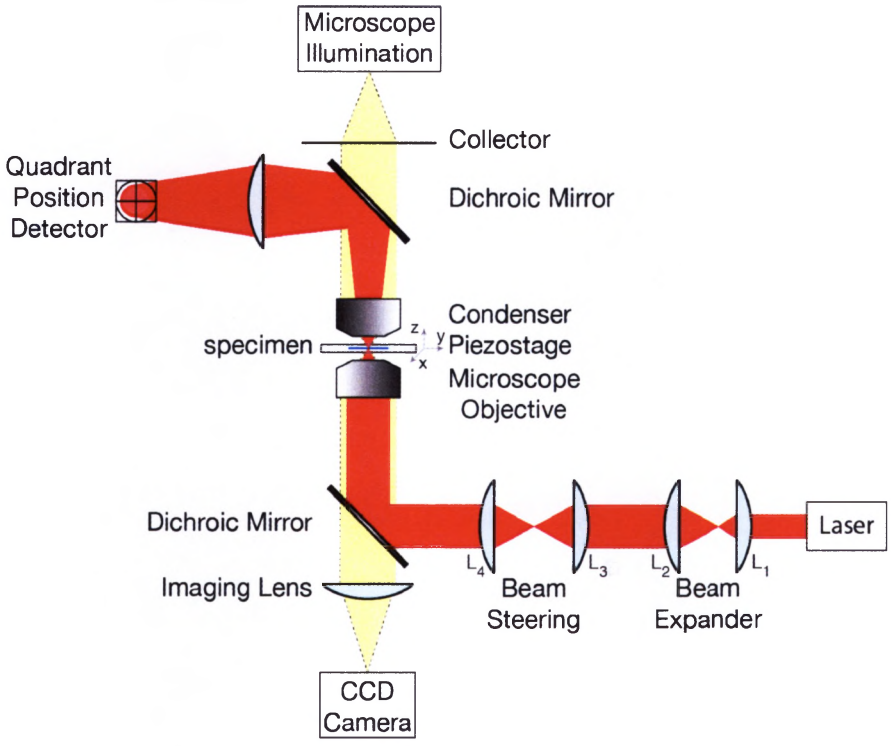

Figure 4.1: Schematic of the experimental setup. An expanded tunable infrared laser beam is coupled into the microscope from the side port. The expanded beam is reflected by a dichroic mirror and tightly focused into the sample dish mounted on a PZ stage.The forward scattered light from the trapped particle is collected by a condenser and then sent to a QPD by reflection from another dichroic mirror. A CCD monitors the trapped particle motion inside a trap and an A/D card is used for data acquisition.

Chapter 5

Chemotaxis in Optical Trapping

Force measurements require precise and accurate calibration of trap parameters. However, direct quantification from the time series or associated power spectral density funcition is intractable in the investigation of bacterial physiology, such as bacterial flagellar motility. Here, we implement an optical tweezers technique to assess the effects of chemical agents on a single bacterial cell. As a proof of principle, the viability of a trapped *Escherichia coli* bacterium is determined by monitoring its flagellar motility in the presence of varying concentrations of ethyl alcohol. We show that the "killing time"of the bacterium can be effectively identified from the correlation statistics of the positional time series recorded from the trap. Our results, which minimize the lethal effects of bacterial photodamage, are consistent with previous reports of ethanol toxicity that used conventional culture-based methods. This

approach can be adapted to study other pairwise combinations of drugs and motile bacteria, especially to measure the response times of single cells with better precision. This work has been published in Ref [37].

5.1 Introduction

Antibiotic resistance poses a serious and growing public health threat that demands continual efforts to identify and synthesize agents with improved antimicrobial activities [41] [42]. In clinical settings, efficient, robust, and sensitive methods of diagnosing antimicrobial resistance and measuring bacterial susceptibility to candidate compounds are critical to both infection control and drug discovery. Traditionally, culture-based methods, such as broth dilutions, have served as the gold standards for antimicrobial susceptibility tests, especially when coupled with miniaturization and automation to achieve rapid processing [43]. Nevertheless, alternative methods that incorporate more recent advances in molecular and non-phenotypic techniques offer potential advantages of improved accuracy, lower cost, reduced sample size, and shorter test time [44] [45] [46]. Here we showcase optical tweezers as a possible tool for direct and accurate assessment of susceptibility at the single-cell level.

Optical tweezers [1] have found many biological, biomedical and atmo-

spheric applications in the past decades [47] [48] [49] [50] [51] [52]. For example, they have been used to manipulate and study whole cells from diverse branches of life and to examine the forces exerted by molecular motors inside these cells; moreover, they have been employed extensively as an effective tool to characterize bacterial chemotaxis and flagellar rotation, revealing new features of bacterial motility previously imperceptible via other approaches [53] [54] [55] [56] [57]. Optical manipulation has also been used previously to investigate the viability of single bacterial cells [58], but the full capability of the technique remains to be explored.

In this work, we employ optical tweezers to examine the lethal effects of varying concentrations of ethyl alcohol on an *E. coli* cell. By tracking and carefully analyzing the dynamics of the trapped bacterium, the "killing time" for different ethanol concentrations can be extracted. Our optical trapping method, which combines Back-Focal-Plane (BFP) interferometry detection [59] [60] with auto-correlation function (ACF) statistics, yielded measurements of ethanol's germicidal effects that agree well with previously published results obtained from culture-based techniques [61] [62]. Thus, our method offers effective and quantitative testing of antibacterial susceptibility at the single-cell level and possesses significant developmental potential for biomedical applications.

5.2 Experimental setup and method

Our home-built Optical Tweezers (OT) system is based on an inverted microscope (Axio Observer D1-Zeiss) which is schematically shown in Fig.5.1. A continuous wave laser beam with TEM_{00} transverse mode (Coherent, $\lambda = 1064\,\text{nm}$) is expanded (represented by L1 and L2 lenses in Fig.5.1) before it is transmitted into the microscope through the side port. The expanded beam is coupled into the optical pathway of the microscope by a Dichroic Mirror (DM1) after which it is tightly focused into the sample chamber using an oil immersion objective lens ($100X$, Zeiss) with Numerical Aperture (NA) of 1.3. The sample chamber is an open-top glass bottom dish (MatTek) mounted on a piezoelectric stage (PI NanoXYZ Piezo Stage), providing positional control of the trap inside the chamber with nanometer resolution. To avoid hydrodynamic effects of the chamber wall [12], the trap is kept about 10 µm away from the bottom of the dish. In order to exclude artifacts that might be caused by photodamage and heating [38] [14] [39], in addition to implementing other optimization techniques [40], the trapping laser power is kept at no more than 40 mW at the sample site. The forward scattered light from the trapped bacterium as well as the direct (un-scattered) light is collected by a condenser lens ($NA = 1.2$). The collected lights are reflected off the optical pathway of the microscope by another Dichroic

Mirror (DM2) and then focused on a Position-Sensitive Detector (PSD) situated at the plane conjugate to the BFP of the condenser. PSD signals are amplified by low-noise preamplifiers (Stanford Research Systems) before being transferred to the computer via an Analog-to-Digital (A/D) card (National Instruments). The PSD positional signals are acquired at a sampling rate of 10 kHz, using a custom-made LabVIEW program. In addition, the trapped bacterium is monitored with a CCD camera. In order to deliver the "drug" under study (ethyl alcohol) into the dish with precise control and minimum hydrodynamic force, a syringe pump is used with a tapered glass capillary (inner diameter of about 2 µm, generated with a micropipette puller (Narishige)).

Generally speaking, bacteria inside the sample chamber can swim, tumble, and move anywhere in the aqueous environment. A bacterium in the trap, however, tends to align itself along the optical axis [63] [64] and is typically driven by two kinds of activities: Brownian motion and flagella-mediated propulsion. Since the latter requires cellular energy, the movement of a dead or metabolically inactive *E. coli* cell in an optical trap can be attributed solely to passive Brownian motion. High temporal resolution of optical tweezers allows for accurate interpretation of these bacterial movements. The positional signal recorded from a trapped bacterium does not seem to have reasonable information; how-

ever, statistical analysis of the signal can deliver valuable information, such as rotation frequency of the flagella and the cell body [56]. Importantly, such analysis can determine whether the trapped bacterium is dead or alive, enabling accurate assessment of the effects of antibacterial agents. It should be noted that the trajectories of a trapped bacterium (PSD signals) are associated with several factors, including trap stiffness, cell size, medium viscosity, and dynamic strength of the bacterium [55] [56] [57]. Different cell sizes can change the corner frequency of PSD and the trap stiffness as well, but such factors should not affect the final results obtained from our autocorrelation analysis described below, because they are based on data obtained from the same single bacterium. Also, the presence of more than one bacterium in the trap can introduce a complicating noise into the PSD signal. To prevent this, a trapped bacterium is moved close to the chamber wall and then gently pressed against the chamber wall, where it changes its orientation. A typical dark-field image of a trapped bacterium under such consideration is shown in Fig.5.1. With this simple procedure we can identify whether there is only one bacterium or multiple bacteria in the trap. For all experiments described below, we took great care to ensure that all data acquired are from single cells in the trap.

In this work, our objective is to trap a single bacterium with optical

tweezers and track its positional changes while introducing an antibacterial agent into the medium, thus allowing us to observe the consequences of bacterial exposure to the chemical agent. To verify the feasibility of our proposed technique, we used different concentrations of ethyl alcohol as the antibacterial agent and obtained the positional time series of a trapped *E. coli* cell after its exposure to alcohol. *E. coli* strain MG1655 was grown in *Luria-Bertani* (*LB*) medium at 37 °C overnight and then diluted ten times into the same medium at 25 °C one hour before experiments. The cultures were further diluted 100 times (to less than 10^5 cells per mL) before addition to the sample chamber to avoid bacterial accumulation at the trap during measurements. Since high concentrations of alcohol may destroy the cell body and cause morphological changes that affect the positional signals, the typical concentrations of ethyl alcohol used in our experiments were 20%, 22.5%, and 25% by total volume (i.e., the volume of the solution inside the chamber plus the volume of added alcohol).

5.3 Experimental results and analysis

In a typical experiment, alcohol is injected gently at a position far away from the trapped bacterium before data acquisition starts. Fig.5.1 shows

the positional time series of a representative bacterium in aqueous solution after exposure to 25% ethanol. The acquired data is divided into 30 s sequences. Fig.5.2(a) shows three representative time sequences at different stages of the acquisition. For each sequence the power spectral density and the Autocorrelation Function (ACF) are calculated; the results are shown in Figs.5.2(b) and 5.2(c), respectively. Although there is no clear difference in the positional time series [Fig.5.2(a)] and its associated power spectral density [Fig. 5.2(b)], their ACF graphs are clearly distinguishable, both from their initial value and their decreasing rate (the slope of the graph) [Fig.5.2(c)]. The inset of Fig. 5.2(c) shows that despite long-time differences, the graphs have a very similar short-time behavior. In a few milliseconds, the ACF of each graph exponentially drops to a slowly varying value. The time constant of this exponential function, which is inversely related to the corner frequency of the relevant power spectrum, is approximately equal for all three graphs.

The first time sequence (black curve) represents the behavior of a living, non-damaged bacterium, while the third sequence (blue curve) mimics pure random Brownian motion, suggesting that at this time the bacterium loses its flagellar activity completely (the behavior of a dead bacterium). Both of the above mentioned cases were checked in separate control experiments. Considering that the ACF of a living bacterium

has the largest area under the graph, we define the normalized ACF, ζ, as the area under the ACF graph divided by that of the living bacterium. Fig.5.2(d) shows the evolution of ζ with time. As time goes by, ζ decreases from its maximum plateau to the minimum baseline (corresponding to the time window of the lethal effect, as illustrated by the aqua-shaded region). We define the time it takes for the normalized ACF to reach half maximum as the "killing time". Apparently this parameter can be used to quantitatively characterize the bacterium's lethal response to alcohol exposure. In other words, the normalized ACF degrades with time, which would not happen for a living bacterium. The lethal response is better characterized by fitting our data to a sigmoidal dose-response function (red solid line in Fig.5.2(d)), with the effective "killing time" of about 130 s (corresponding to the time at half maximum, marked by dotted line).

We expected that lower concentrations of alcohol would lead to a longer killing time. To validate this quantitatively, other concentrations (22.5% and 20%) were also tested. In addition, a control experiment was performed in which no alcohol was added (0%), to eliminate the possibility of lethal effects due to heating and bacterial photodamage [38] [14] [39]. Representative experimental results are summarized in Fig.5.3, which shows that the measured killing time values become larger when the

alcohol concentration is lowered. For autocorrelation analysis and comparison, it is crucial to avoid any other unwanted disturbance in the time signal, such as bacterial tumbling or the trapping of multiple cells. Thus, we repeated the experiments with different, randomly chosen bacteria from ten independent samples at each alcohol concentration. The average killing times for 25%, 22.5%, and 20% ethyl alcohol, as shown at half maximum of ζ by red dotted lines in Fig.5.3, are 130 ± 20 s, 230 ± 35 s, and 550 ± 50 s, respectively. (The standard deviations are extracted from measurements of ten independent samples.) Our results demonstrate clearly that higher concentrations of alcohol lead to faster killing and that such killing is not due to photodamage, as the bacterium remains alive for the whole data acquisition period (about 550 s) when no alcohol is added. In order to confirm the reliability of the current technique, we have also performed a series of experiments with another *E. coli* strain ($KS272$) and obtained similar results of alcohol concentration dependence.

5.4 Conclusion

We have employed an optical tweezers to study the toxic effect of an antimicrobial agent on single bacterial cells. We demonstrated that the

"killing time" of an *E. coli* cell coming into contact with ethanol in aqueous solution can be calculated from statistical analysis of its positional time signals, which allows distinction of bacterial flagellar motion from random Brownian motion. This technique may be further optimized to develop an effective tool for studying bacterium-drug interactions.

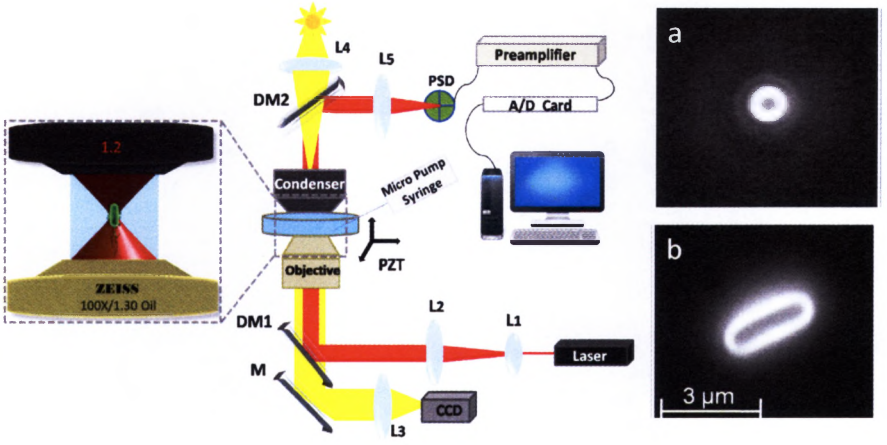

Figure 5.1: Schematic of the experimental setup. An expanded 1064 nm laser beam is coupled into the microscope from the side port with a Dichroic Mirror (DM1). The expanded beam is tightly focused into the sample dish mounted on piezoelectric transducer (PZT).The forward scattered light from the trapped object is first collected by a condenser lens and then sent to a Position-Sensitive Detector (PSD) by reflection from another Dichroic Mirror (DM2). Low-noise preamplifiers and A/D card are used for signal conditioning and data acquisition. A microsyringe pump is used for delivering alcohol into the dish. The insert on the left illustrates a zoomed view of a single bacterium trapped by the optical tweezers. Insets on the right show typical dark-field images of an *E. coli* bacterium trapped by an optical tweezers. (a) When the bacterium is trapped inside the sample chamber, i.e., in bulk, the bacterium aligns itself along the laser beam axis, such that only a transverse projection is seen; (b) when it is gently pushed against the chamber wall, the cell changes orientation, showing clearly the entire rod-shaped body.

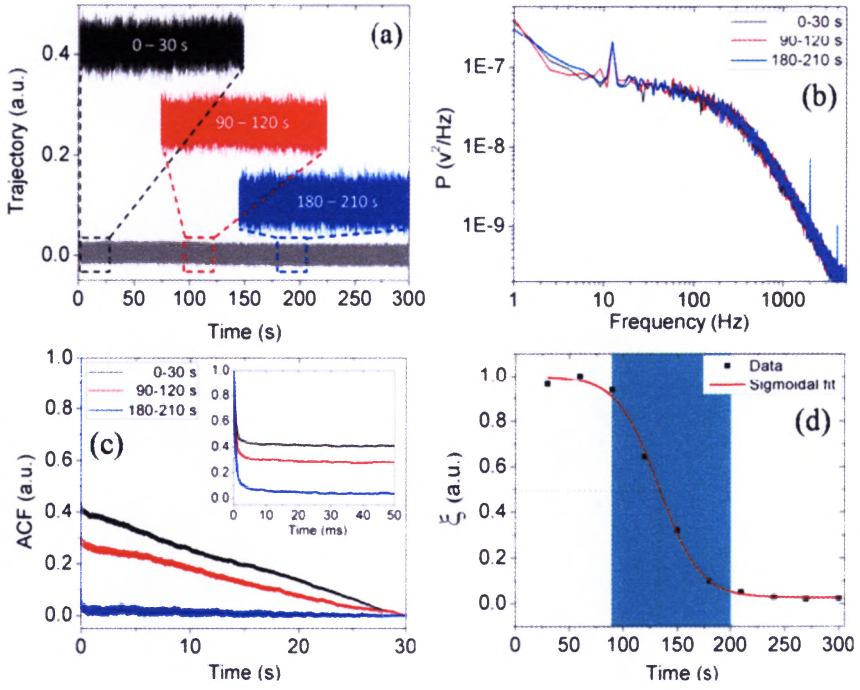

Figure 5.2: (a) Positional time series (trajectory) of a trapped bacterium in the lateral direction for 300 s (bottom trace, gray) after introducing 25% ethyl alcohol. Three different sections, at intervals of 0 to 30 s, 90 to 120 s and 180 to 210 s, were expanded and represented in black, red and blue, respectively. (b) Calculated power spectral density and (c) Autocorrelation function (ACF) corresponding to the three sections in (a). (d) Normalized ACF (ζ) calculated for each 30 s time series obtained at different times after adding the alcohol. The points are from calculation of measured data, while the red line is the sigmoidal dose-response-function fit.

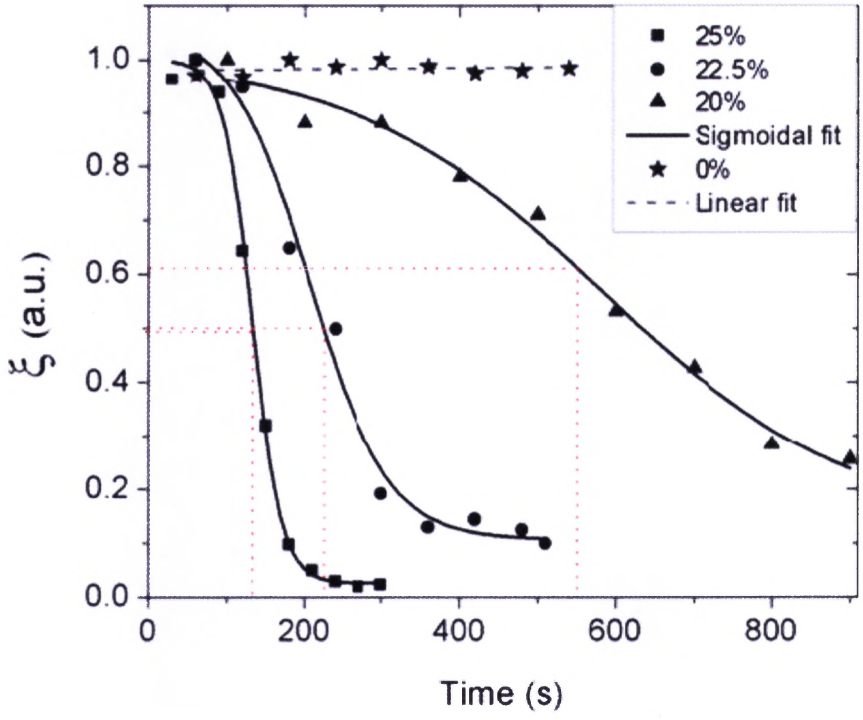

Figure 5.3: Normalized ACF (ζ) vs. time for different alcohol concentrations. The killing times for 25%, 22.5%, and 20% concentrations are determined to be 130 s, 230 s, and 550 s, respectively, and these are representative killing times of a single cell. For each concentration, measurements were done for at least 10 cells, yielding similar results with standard deviations. When no alcohol (0%) is added, the normalized ACF (ζ) does not change appreciably with time, indicating that the lethal effect is not due to photodamage.

Chapter 6

Phototaxis in Optical Trapping

Optical tweezers provide a unique means for manipulation and control over biological objects at the single cell level. However, the trapping laser beam, especially in the visible region, typically induces photodamage to the trapped cell. We examine the photodamage effect of a visible (532 nm) trapping beam on *Escherichia coli* cells using dark-field microscopy. We observe that under the influence of the trapping beam, not only do the cells experience cross-sectional area shrinkage due to laser radiation, but more surprisingly, such photodamage-induced cells shrivel strongly depending on the cell culture media. Specifically, we compared average characteristic shrinkage time constants for decreasing cross area of trapped bacteria grown in different media, e.g., *lysogeny broth* (*LB*) and *tryptone yeast* (*TY*) media under the same condition of an optical trapping setting, and found that the bacteria grown in *TY*

medium have larger average shrinkage time constant than those grown in LB medium, which indicates that the bacteria grown in TY medium may build up more rigid membrane structure and are more immune to laser-induced damage effect compared with those grown in LB medium. Furthermore, cross-area-dependent laser-induced damage can be applied to study the bacteria-bacteria and bacteria-drug interaction.

6.1 Introduction

Originating from the optical radiation pressure, the focused coherent light beam is able to grab, manipulate, and control microscopic objects [1]. Optical tweezers have brought numerous successful applications of manipulating and controlling microscopic objects without mechanical contact and direct force measurement. In biological studies, it has been demonstrated that the trapping of viruses and bacteria [48], yeast cells, human blood cells, protozoa, various algae and plants cells [47], sperm cells [65], and the chromosomes [65]. It has successfully sorted cells [66], measured forces generated by sperm cell [65] and motor molecules driving mitochondrion along microtubules [67] [7], characterized the elasticity of bacteria flagella [53]. In general, the light source used to trap biological samples are in near infrared and infrared regions. Intuitively, photons

with longer wavelengths carry less energy compared to those in shorter wavelengths based on the Planck equation and biological specimens have lower absorption in such wavelengths. However, no matter which wavelengths are chosen to be laser sources of optical tweezers, at the trapping point, the intense trapping laser beam somehow causes optical induced damage (photodamage) on trapped objects [14]. For instance, heavy absorption of pigments from the visible region and surrounding solutions, such as water, from the far-infrared region may cause interruption of normal cell functioning [68]. In addition, free oxygen radicals are generated in aqueous solutions and cause the damage on specimens. In this work, we concentrate on the photodamage effect of visible trapping laser beams and quantitatively examine how strong bacteria grown in different media may resist the effect of intensely focused laser beams.

In microbiology, the bacteria-bacteria interaction, bacteria swimming can be studied using optical tweezers [56] [57]. The infrared (IR) beam is usually used to minimize the photodamage on biological sample. The IR laser excites molecular oxygen in aqueous solutions to generate reactive oxygen species, which inevitably induces damage to nucleic acids [69]. The more energy a single photon carries, the more damage it will cause on the biological sample. However, the visible beam with higher photon energy in some instances provide better applications, such as simultane-

ous excitation of fluorescence. How the green beam will cause damage in laser tweezers experiment has not been quantitatively investigated. We observed that under dark-field microscopy, the bacterium experiences a size shrinkage in the optical tweezers. We will quantify the laser induced photodamage on the single cell level by characterization of the cell size change on different bacteria.

In this work, a dark-field microscope allows us to monitor instantaneous behaviors of *Escherichia coli* under optical tweezers. Through image analysis of cross sectional areas of trapped cells, we discover that the cells experience size shrinkage and this shrivel strongly depends on the cell growth condition, such as culture media.

6.2 Experimental setup and method

The optical tweezers are built on a commercial inverted microscope (Zeiss Axio Observer D1) working in dark-field mode [Fig.6.1]. A solid-state laser (CW, 532 nm) is used as the laser source for our trapping experiment. The beam is expanded (by L1 and L2 in Fig.6.1) and steered (by L3 in Fig.6.1) before being directed into the microscope. Such converged beam is collimated by the built-in tube lens (L4 in Fig.6.1) and further focused to a diffraction limited spot by a high numerical aperture objec-

tive (EC Plan-Neofluar, $100X$, $NA = 1.3$). The trapping position can be controlled in three dimensions by the steering lens (L3). The bacteria sample under study is sandwiched between two microscope slides glued by double-sided tape. The glass slide is further mounted on a piezoelectric translational stage (PI, NanoXYZ) for fine control of the position. A dark-field condenser selectively passes a ring beam for illumination of the microscopic sample, while the straight light is further blocked by the trapping objective lens, allowing only the scattered light being collected by the imaging system. The dark-field images have a black background, while the bacterium appears as a bright object with sharp edge due to light scattering. Such dark-field images recorded the changing of morphology a single bacterium, and thus are suitable for the investigation of the photodamage under optical tweezers.

The bacterium has an average refractive index slightly greater than that of background media of which the majority is water. This tiny contrast of refractive index makes the bacterium difficult to be clearly visualized under standard optical microscope. The fluorescence microscope may provide clear images; however, the bacterium needs to be stained with a certain fluorophore, and the photodamage on the fluorophore may further deteriorate the bacterium structure. We take advantage of the dark-field microscope, which could enhance the imaging of living bio-

logical sample without staining. Briefly, the illumination light of the dark-field microscope is blocked in the center by a patch stop inside the condenser, and the peripheral rays are further blocked by a compensating iris inside the objective lens. Consequently, the background of the dark-field microscope is purely dark, however, if the biological sample is within the focal plane, the scattered light will have spatial frequency different from the incident illumination, making the sample visible in the dark background. The optical tweezers employ a high NA objective lens for three-dimensional confinement of a bacterium, correspondingly, the NA of the condenser lens (Zeiss cardioid-designed Ultra condenser 1.2/1.4) should match that of the trapping lens. Although the lack of destructive interference with undiffracted light at the image plane cannot yield structural details in the specimen compared to phase contrast microscopy, dark-field microscopy is a perfect tool to study the photodamage effect of an optical tweezer in our study without considering the possibility of damaging the phase ring of an objective lens of phase contrast microscopy, especially at high power photodamage investigation. To achieve the maximum detection of cross sectional area of a bacterium dark-field image, a trapped bacterium is gently moved upward and pressed against the chamber ceiling where it changes its orientation till bacterial membranes have clear contours as Fig.6.1(b) shows; then,

the rest of experiments are performed at a similar depth inside the chamber. A series of dark-field images are recorded for further analysis of the dynamics of trapped bacterium by the calculating the cross-sectional area.

The bacterium held in the laser trap exhibits various behaviors, including the swimming, tumbling, and photodamage [55] [37]. The major objective is to characterize the photodamage by monitoring the morphological change under dark-field microscopy. To demonstrate this method, the E. coli strain $MG1655$ is prepared in two different media, *Lysogeny Broth* (LB) and *Tryptone Yeast* (TY), at 37 °C overnight. One aliquot of 1 mL cell culture is then resuspended with 3 mL fresh media at 25 °C to improve the bacterial motility.

To prevent bacteria accumulation during the optical tweezer experiment, before damaging with the green laser, cell sample is further suspended into water to keep cell concentration at 10^5 to 10^6 cells per mL. Each time, a single bacterium was trapped and brought close to the chamber ceiling for better characterization of the size change. The dark-field images were acquired in real time to evaluate the dynamical change of the cross area.

While trapping with the green laser, the bacterium enters the trap and tends to align along the optical axis, the origination of the trapped bac-

teria is forced to be normal to the optical axis to achieve the maximum detection of the cross section of the bacterium. Then, the video is recorded by a Thorlabs CCD camera while it is trapped. The experiment is performed in the same manner for bacteria grown in both media. Then, cross sectional areas of dark-field images are calculated and average shrinkage time constants are compared for decreasing cross-sectional area of *E. coli* grown in different media. Three independent colony-forming unit (CFU) experiments are further performed to verify that the visible laser causes the damage effect on the bacteria. The collimated 532 nm laser, with beam waist about 2 cm and power density about 200 $\mathrm{W\,cm^{-2}}$, blasts 1 mL of the bacteria suspension with cell concentration about 8×10^7 cells per mL for 1 h on a petri-dish. We recover the laser treated/untreated bacteria suspension overnight on agar plates for a concentration gradient.

6.3 Experimental results and analysis

E. coli bacteria grown in *LB* media are trapped by our laser tweezers instrument. The dark-field microscope monitors the dynamical images of the trapped bacterium brought close to the coverslide. The analysis of cross-sectional area of more than 50% of the trapped bacteria shows

an exponential decaying trend under the optical tweezers with a power of 70 mW at wavelength of 532 nm [Fig.6.2(a)]. About 70% of trapped bacteria show a square wave signal which indicates that the bacterium is dancing because of the possible transformation between swimming and tumbling in the laser tweezers [Fig.6.2(b)]. When the trapping laser is switched to an infrared beam (IR, wavelength of 1064 nm) with even stronger power (100 mW), the cross area of the trapped bacteria does not change with time for most of them [Fig.6.2(c)]. Interestingly, we found the bacterial dancing signal apparently to be a step function for those bacteria that may undergo the transformation [Fig.6.2(d)]. The cross area shrinking under visible beam focus may indicate an irreversible damage on cell structure, such as cell membranes, etc. And this event is immune to the IR beam. The exponentially decaying curve with the 532 nm laser beam was further fitted with a model to determine the characteristic shrinkage time constant for the decaying, $\frac{A(t)}{A_0} = a \exp\left(\frac{t}{\tau}\right) + b$, where $A(t)$ and A_0 are the cross-sectional areas at $t = 0$ s and time t, a and b are dimensionless factors and τ is the characteristic shrinkage time constant. The characteristic shrinkage time constant for the bacterium under the 532 nm laser trap is 57.73 s [Fig.6.2(a)], while the bacterium in the IR trap does not experience size shrinkage. The different behavior under laser tweezers with 532 nm and 1064 nm indicate that the 532 nm

beam is more harmful to biological samples than the IR beam.

Apart from tightly fixed bacteria experiencing morphological changes, those bacteria held in the laser trap away from the glass surface show this very interesting dancing signal [Figs.6.2(b) & (d)]. Alive bacterium in the aqueous environment swims or tumbles due to the strong force driven by flagella bundle [70] [71] [72]. This type of signal appears in both cases with visible and IR beams, which may indicate the bacterium may undergo the transformation of swimming and tumbling and tend to move away from the confinement of the glass slide. The bacterial signal under the IR beam is a resemble step function compared to the bacterium trapped with the visible beam, which shows that the laser-induced damage effect indeed takes place in the visible beam trap. Prolate particles with large aspect ratio align the long axis with the beam propagation direction in the laser trap [73] [74]. The geometry of bacterium can be well approximated to be a prolate ellipsoid. The trapped bacterium also aligns itself along the optical axis [64]. The tumbling enables the configuration of a bacterium to be flipped down in the transverse plane. The competing balance of such two spatial configurations brings about the two-state hopping of the cross area analysis. The hopping is more apparent on the bacterium trapped with the IR beam since the photodamage is insignificant compared to the visible beam. In contrast, the hopping

signal should not appear in the bacterium without flagella, e.g., *Sinorhizobium meliloti*, etc., or less transformation of swimming and tumbling. However, a further investigation is required.

A biological system is a very complex system where many parameters jointly determine the behavior for even a single bacterium. The laser-induced damage of the bacteria will vary from bacterium to bacterium. To get a better understanding of how the bacteria grown in a different buffer is damaged by the visible beam, we performed a series of experiments to accumulate enough statistics for evaluation of the laser-induced damage effect. The characteristic shrinkage time constant for the photodamage was determined with each trace. The histogram of the characteristic shrinkage time constants for the bacteria grown in LB buffer and trapped with 70 mW green laser is shown in Fig.6.3(a). The histogram of characteristic shrinkage time constants fits well with an exponential curve which determines the average characteristic shrinkage time of 89 s for the bacterium to experience significant laser-induced damage effect in the visible beam.

Fig.6.3 shows statistical analysis of characteristic shrinkage time constants of decreasing cross area for bacteria grown in LB and TY media, while they are trapping and damaging by nearly 70 mW 532 nm green beam. Once again, the exponential decay distribution of characteristic

time constants of the bacteria from different growth media is chosen to be the probability density function, $N = c \exp\left(\frac{\tau}{T}\right) + d$, where N is the number of the characteristic shrinkage time constant τ which falls in a certain time range, c and d are other dimensionless factors and T is the average shrinkage time constant for decreasing cross area of trapped bacteria grown in a medium. The histogram in Fig.6.3(a) shows the distribution of characteristic shrinkage time constants for decreasing cross area of trapped *E.coli* grown in *LB* media and the average shrinkage time constant for the decrease is found to be about 89 s. Comparing with the average time constant for the decrease in cross area of trapped *E.coli* grown in *TY* media, that is 193 s shown in Fig.6.3(b), the bacteria grown in *TY* media has been damaged less than those grown in *LB* media. In other words, the bacteria grown in *TY* media have more strength to resist laser-induced damage effect compared to those grown in *LB* media.

To verify the results from optical trapping of the 532 nm beam with power density flux over $1 \times 10^{10}\,\mathrm{W\,s^2\,cm^{-1}}$ at the focal plane, the cells are blasted with the collimated 532 nm beam on petri-dishes at power density flux about $1 \times 10^{6}\,\mathrm{W\,s^2\,cm^{-1}}$. Table. 1 shows the average CFU calculation for bacteria grown in different media with no- and post-damage by the collimated 532 nm laser beam. The analysis of *E. coli*

	Average CFU/mL of bacteria grown in *LB*	Average CFU/mL of bacteria grown in *TY*
Negative Control	2.2×10^8	3.0×10^8
Treatment with 532 nm	6.2×10^7	1.3×10^8
% Difference between Negative Control and Treatment with 532 nm	28.2%	41.5%
T-test	0.004	0.353

Table 6.1: Colony-forming unit results for blasting *E. Coli* grown in *LB* and *TY* media by the collimated 532 nm beam for 1 h. The percent difference for bacteria grown in *LB* medium is 28.2% with p-value 0.004 in the two-tailed student's t-test. The percent difference for bacteria grown in *TY* medium is 41.5% with p-value 0.353 in the two-tailed student's t-test.

grown in *LB* medium shows a 28.2% decrease after being blasting by the 532 nm beam for 1 h with p-value of 0.004 in the students t-test, which indicates that a significant reduction occurs in those bacteria grown in *LB* medium even at such low power density flux. In contrast, although 41.5% difference between negative control and 532 nm laser treatment is yielded for bacteria grown in *TY* medium, the p-value of the t-test is 0.353 and indicates that this difference does not have a statistical significance. In other words, the laser-induced damage effect is not significant for those bacteria grown in *TY* medium. Overall, the CFU calculation agrees with the results that are obtained from dark-field optical trapping. The reason might be the focused laser beam cause an additional stress to

cell membranes which leads the interruption of normal cell functioning and affect cell division.

6.4 Conclusion

In summary, we have quantified the laser-induced damage effect on bacteria in optical tweezers by analyzing characteristic cross area shrinkage time constants under dark-field microscopy. The bacteria grown in different buffer solutions show different response in the tightly focused beam, in particular, the *E.coli* grown in *LB* medium are less resistant to photodamage, while those grown in *TY* medium are more stable under the exposure of high intensity visible beams. Furthermore, we could apply this technique to another bacterial species, such as *S. meliloti*, to examine whether bacteria grown in *TY* media always have more strength to resist photodamage than those grown in *LB* media.

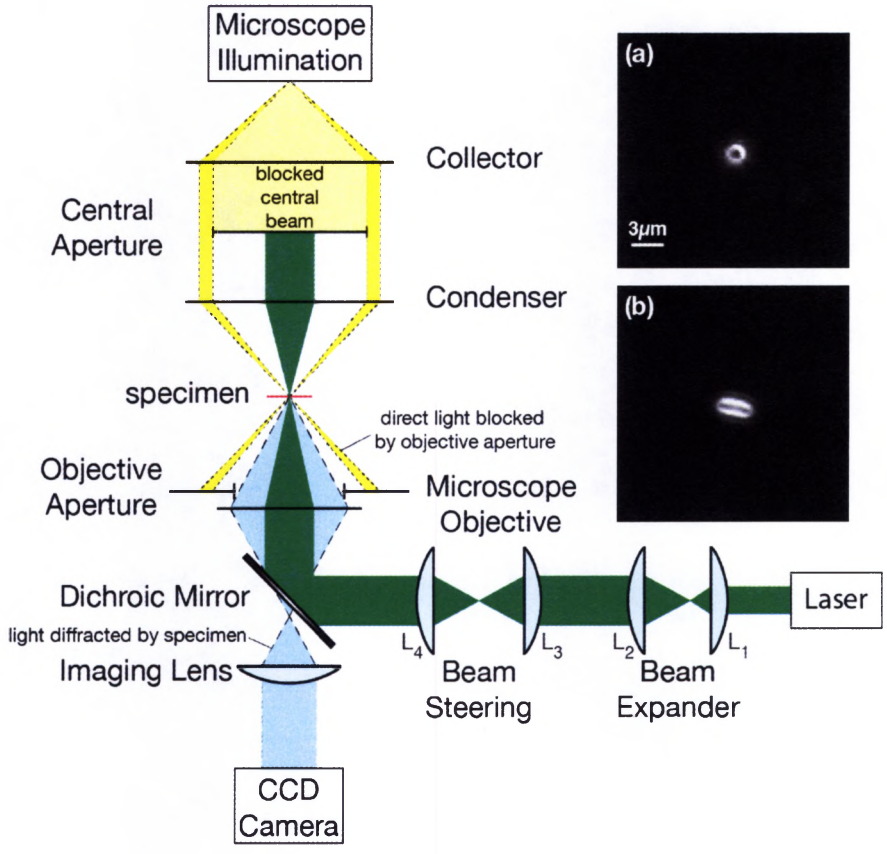

Figure 6.1: Schematic of optical tweezers combined with dark-field microscopy. a) Dark-field image of a trapped bacterium experiencing a three-dimensional confinement in optical tweezers. b) Dark-field image of a trapped bacterium brought closed to microscope side by the optical tweezers experiencing two-dimensional confinement.

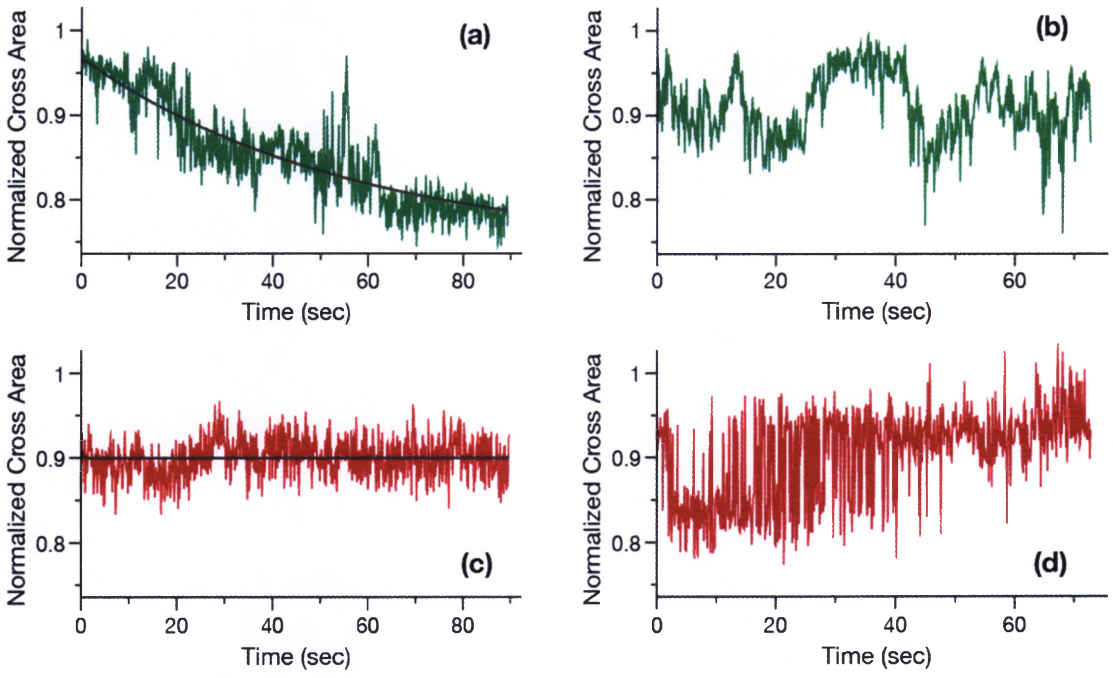

Figure 6.2: a) The normalized cross-sectional area of a bacterium trapped by a 532 nm beam. The power of the trapping beam (532 nm) is about 70 mW at the focal plane. b) A square wave hopping signal of the trapped bacterium under the 532 nm beam appears in the cross area calculation. c) The normalized cross sectional area of a bacterium trapped by a 1064 nm beam. The power of the trapping beam (1064 nm) is about 100 mW at the focal plane. d) A step function hopping signal of the trapped bacterium under the 1064 nm beam appears in the similar calculation.

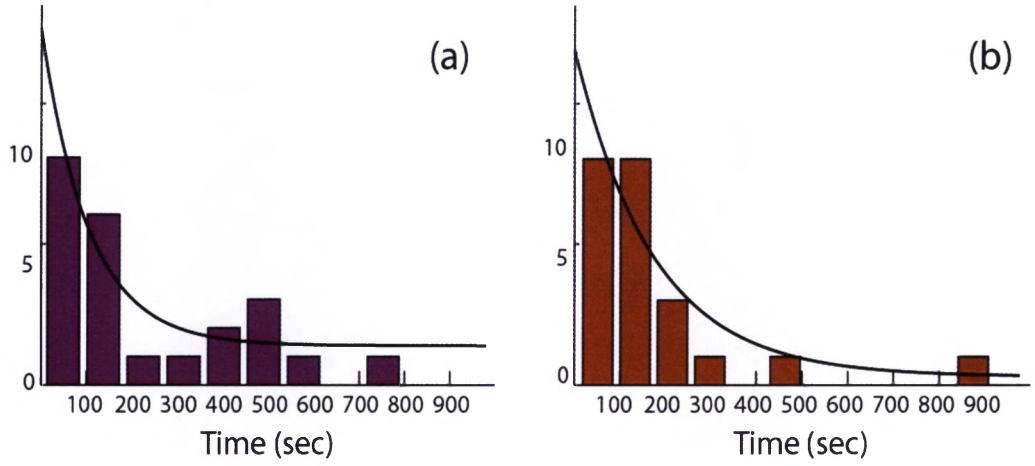

Figure 6.3: Histograms of characteristic shrinkage time constants τ of trapped *E. coli* grown a) in *LB* medium and b) in *TY* medium. The average shrinkage time constant T are 89 s and 193 s respectively for bacteria grown in *LB* and *TY* media.

Chapter 7

Conclusion

From analytical calculations of optical gradient and scattering forces to experimental measurements of those forces acting on an optically trapped particle, optical trapping is capable of detecting nanometer displacements, manipulating microscopic objects and measuring piconewton forces. Furthermore, it has been applied in various fields. Involving concepts in microscopy, optics and laser techniques, an optical trap usually starts with modifying a commercial microscope. A laser source is expanded, steered then coupled into and out of the microscope with a pair of dichroic mirrors. An objective lens with a high NA is mandatory to create a three-dimensional optical confinement. With imaging capabilities of the microscope, videos and frames of the trapped particle motion can be used in the analysis and determination of trap parameters, such as the trap stiffness and the drag coefficient. In the mean while, the

forward scattered light from the trapped particle is collected by a condenser and then sent to a position sensing detector for the same purpose. A dynamical position control system is required for such an instrument to achieve the greatest sensitivity, stability and signal-to-noise ratio. In terms of calibration methods that are required a harmonic trapping potential, the Equipartition theorem method is the simplest method to calibrate an optical trap without knowing a particle shape, its trapping depth and the viscosity of the background medium. With identical bandwidth on a detection system but improved accuracy, the power spectral density analysis is the most common method used in the calibration of Brownian motion in a harmonic potential. However, the most direct method for the calibration is the viscous drag force method which an external drag force is generated by controlling a piezoelectric stage and/or varying the medium velocity. Since direct quantification from the time series or associated power spectral density function from a trapped bacterium motion is intractable, a statistical method involving the analysis of autocorrelation function for the bacterial motion has been used for the investigation of bacterial physiology. In the presence of alcohol at different concentrations, the corresponding "killing time" of *Escherichia coli* that is measured by optical trapping is consistent with previous reports of ethanol toxicity that used conventional culture-based methods

even though the associated corner frequencies do not have significant difference. Because a tightly focused beam is used to trapped particles, implementing dark-field illumination with optical trapping, cross areas of trapped *E. coli* by 532 nm shrinks significantly. More significantly, the shrinkage rate of the bacterial cross area is strongly related to bacterial growth conditions, while the photon-induced damage by optical trapping has been verified by conventional colony-forming unit calculation. Overall, optical trapping provides precise and accurate measurement of nanometer displacement and piconewton forces. However, it has to be considered carefully prior to and during the usage due to instrument design limitations, photon-induced damage to the specimen, research budget, etc.

Appendix A

Essential Calculations

A.1 Force Calculations

A.1.1 Rayleigh Regime

In case where the dimension of a perfect spherical dielectric object with radius a is within an order of magnitude of the trapping beam wavelength, light rays cannot be traced and particles can be treated as electric dipoles in an electric field. Thus, forces are calculated based on wave-optics theory [75]. The Gaussian beam theory for an $x-$polarized

light wave is

$$\widetilde{\vec{E}}(\vec{r}) = \hat{x}\widetilde{E}(\vec{r}),$$
$$= \hat{x}E_0 \frac{ikw_0^2}{ikw_0^2 + 2z} \exp(-ikz) \exp\left(-i\frac{2kz(x^2+y^2)}{(kw_0^2)^2 + (2z)^2}\right) \exp\left(-\frac{(kw_0)^2(x^2+y^2)}{(kw_0^2)^2 + (2z)^2}\right),$$

and

$$\widetilde{\vec{H}}(\vec{r}) = \hat{y}\widetilde{H}(\vec{r}),$$

where w_0 is the beam waist and k is the wavenumber. Then, expressing the real parts of the fields, we may obtain

$$\vec{E}(\vec{r}, t) = Re\left(\widetilde{\vec{E}}(\vec{r}) \exp(i\omega t)\right),$$

and

$$\vec{H}(\vec{r}, t) = Re\left(\widetilde{\vec{H}}(\vec{r}) \exp(i\omega t)\right),$$

where ω is the angular frequency of the light wave. Then, the Poynting vector of an x-polarized light wave is defined as:

$$\begin{aligned}\vec{S}(\vec{r},t) &\equiv \vec{E}(\vec{r},t) \times \vec{H}(\vec{r},t), \\ &= Re\left(\widetilde{\vec{E}}(\vec{r})\exp(i\omega t)\right) \times Re\left(\widetilde{\vec{H}}(\vec{r})\exp(i\omega t)\right), \\ &= \frac{1}{2}\left(Re\left(\widetilde{\vec{E}}(\vec{r}) \times \widetilde{\vec{H}}(\vec{r})\right) + Re\left(\widetilde{\vec{E}}(\vec{r}) \times \widetilde{\hat{H}}(\hat{r})\exp(2i\omega t)\right)\right).\end{aligned}$$

The intensity of an $x-$polarized light wave is defined as:

$$\begin{aligned}\vec{I}(\vec{r}) &\equiv \left\langle \vec{S}(\vec{r},t)\right\rangle_T, \\ &= \frac{1}{2}Re\left(\widetilde{\vec{E}}(\vec{r}) \times \widetilde{\vec{H}} * (\vec{r})\right), \\ &= \hat{z}\frac{m\varepsilon_0 c}{2}\left|\vec{E}(\vec{r})\right|^2, \\ &= \hat{z}I(\vec{r}),\end{aligned}$$

where c is the speed of light, m is the ratio of refractive indices of the trapped particle and the background medium and

$$I(\vec{r}) = \left(\frac{2P}{\pi w_0^2}\right)\frac{1}{1+\left(\frac{2z}{kw_0^2}\right)^2}\exp\left(-\frac{2\left(\left(\frac{x}{w_0}\right)^2+\left(\frac{y}{w_0}\right)^2\right)}{1+\left(\frac{2z}{kw_0^2}\right)^2}\right),$$

which $P = \frac{\pi w_0^2 n_2 \varepsilon_0 c E_0^2}{4}$ is the power of an $x-$polarized light wave. The dipole moment $\vec{p}(\vec{r},t)$ of a perfect spherical dielectric object with radius a in the instantaneous electric field of $\vec{E}(\vec{r},t)$ is

$$\begin{aligned}\vec{p}(\vec{r},t) &= 4\pi\varepsilon_2 a^3 \left(\frac{\varepsilon_1-\varepsilon_2}{\varepsilon_1+2\varepsilon_2}\right)\vec{E}(\vec{r},t), \\ &= 4\pi\varepsilon_0 n_2^2 a^3 \left(\frac{m^2-1}{m^2+2}\right)\vec{E}(\vec{r},t).\end{aligned}$$

Scattering Force

The scattering force is

$$\begin{aligned}\vec{F}_{\text{scat}}(\vec{r}) &= \frac{C_{pr}\left\langle \vec{S}(\vec{r},t)\right\rangle_T}{\frac{c}{n_2}}, \\ &= \hat{z}\frac{n_2}{c}C_{pr}I(\vec{r}),\end{aligned}$$

where C_{pr} is the cross section for the radiation pressure of the particles and expressed as:

$$C_{\text{pr}} = \frac{8}{3}\pi(ak)^4 a^2\left(\frac{m^2-1}{m^2+2}\right)^2.$$

Then, the scattering force becomes

$$\vec{F}_{\text{scat}}(\vec{r}) = \hat{z}\frac{n_2}{c}\frac{8}{3}\pi(ak)^4 a^2\left(\frac{m^2-1}{m^2+2}\right)^2 I(\vec{r}).$$

Gradient Force

An instantaneous gradient force is

$$\begin{aligned}\vec{F}_{\text{grad}}(\vec{r},t) &= \left(\vec{p}(\vec{r},t)\cdot\vec{\nabla}\right)\vec{E}(\vec{r},t),\\ &= 4\pi\varepsilon_0 n_2^2 a^3\left(\frac{m^2-1}{m^2+2}\right)\frac{1}{2}\vec{\nabla}E^2(\vec{r},t).\end{aligned}$$

Then, a time-averaged gradient force is

$$\begin{aligned}\vec{F}_{\text{grad}}(\vec{r}) &= \left\langle \vec{F}_{grad}(\vec{r},t)\right\rangle_T,\\ &= 2\pi\varepsilon_0 n_2^2 a^3\left(\frac{m^2-1}{m^2+2}\right)\vec{\nabla}\left\langle E^2(\vec{r},t)\right\rangle_T,\\ &= \pi\varepsilon_0 n_2^2 a^3\left(\frac{m^2-1}{m^2+2}\right)\vec{\nabla}\left|E(\vec{r},t)\right|^2,\\ &= \frac{2\pi n_2 a^3}{c}\left(\frac{m^2-1}{m^2+2}\right)\vec{\nabla}I(\vec{r}).\end{aligned}$$

The gradient force on each component is

$$\vec{F}_{\text{grad},x}(\vec{r}) = \hat{x}\frac{2\pi n_2 a^3}{c}\left(\frac{m^2-1}{m^2+2}\right)\frac{\frac{4x}{w_0^2}}{1+\left(\frac{2z}{kw_0^2}\right)^2}\frac{I(\vec{r})}{2},$$

$$\vec{F}_{\text{grad},y}(\vec{r}) = \hat{y}\frac{2\pi n_2 a^3}{c}\left(\frac{m^2-1}{m^2+2}\right)\frac{\frac{4y}{w_0^2}}{1+\left(\frac{2z}{kw_0^2}\right)^2}\frac{I(\vec{r})}{2},$$

and

$$\vec{F}_{\text{grad},z}\left(\vec{r}\right) = \hat{z}\frac{2\pi n_2 a^3}{c}\left(\frac{m^2-1}{m^2+2}\right)\frac{\frac{8z}{\left(kw_0^2\right)^2}}{1+\left(\frac{2z}{kw_0^2}\right)^2}\left(1-\frac{2\left(\left(\frac{x}{w_0}\right)^2+\left(\frac{y}{w_0}\right)^2\right)}{1+\left(\frac{2z}{kw_0^2}\right)^2}\right)I\left(\vec{r}\right).$$

A.1.2 Mie Regime

In case where the dimension of a spherical dielectric particle with radius a is much greater than the wavelength of the trapping beam, trapping forces can be calculated based on ray-optics theory. Assume a ray of power P hits the particle at an angle θ where it partially reflects and refracts, giving rise to a series of scattered rays of power PR, PT^2, PT^2R, ..., PT^2R^n, ..., where R and T are the Fresnel reflection and transmission coefficients of the surface at θ. Denote θ and θ_{refr} as the angles of incidence and refraction, and the angles relative to the incident ray is $\pi + 2\theta$, α, $\alpha + \beta$, ..., $\alpha + n\beta$, ..., where $\alpha = 2\theta - 2\theta_{\text{refr}}$ and $\beta = \pi - 2\theta_{\text{refr}}$. Based on geometrical optics, the scattering and gradient forces generated by a single ray is

$$f_{\text{scat}} = \frac{n_2 P}{c} - \frac{n_2 P}{c}\left(\cos\left(\pi+2\theta\right) + \sum_{n=0}^{\infty} T^2 R^n \cos\left(\alpha+n\beta\right)\right),$$

and

$$f_{\text{grad}} = 0 - \frac{n_2 P}{c}\left(\sin(\pi + 2\theta) + \sum_{n=0}^{\infty} T^2 R^n \sin(\alpha + n\beta)\right),$$

respectively. Applying trigonometric identities,

$$\begin{aligned}\sum_{n=0}^{\infty} R^n \cos(\alpha + n\beta) &= \sum_{n=0}^{\infty} R^n (\cos\alpha\cos n\beta - \sin\alpha\sin n\beta), \\ &= \cos\alpha \sum_{n=0}^{\infty} R^n \cos n\beta - \sin\alpha \sum_{n=0}^{\infty} R^n \sin n\beta.\end{aligned}$$

Applying Eq. Eq. 1.447.1&2 in Ref. [76],

$$\begin{aligned}\sum_{n=0}^{\infty} R^n \cos(\alpha + n\beta) &= \cos\alpha \times \frac{1 - R\cos\beta}{1 - 2R\cos\beta + R^2} - \sin\alpha \times \frac{R\sin\beta}{1 - 2R\cos\beta + R^2}, \\ &= \frac{\cos\alpha - R(\cos\alpha\cos\beta + \sin\alpha\sin\beta)}{1 - 2R\cos\beta + R^2}, \\ &= \frac{\cos\alpha - R\cos(\alpha - \beta)}{1 - 2R\cos\beta + R^2}. \end{aligned} \tag{A.1}$$

Applying $\cos(\pi + 2\theta) = -\cos 2\theta$ and substituting Eq.$A.1$ into f_{scat}, the scattering force generated by a single ray is expressed as:

$$\begin{aligned}
f_{\text{scat}} &= \frac{n_2 P}{c} - \frac{n_2 P}{c}\left(-\cos 2\theta + T^2 \times \frac{\cos\alpha - R\cos(\alpha-\beta)}{1-2R\cos\beta+R^2}\right), \\
&= \frac{n_2 P}{c}\left(1+\cos 2\theta - \frac{T^2(\cos\alpha - R\cos(\alpha-\beta))}{1-2R\cos\beta+R^2}\right), \\
&= \frac{n_2 P}{c}\left(1+\cos 2\theta - \frac{T^2(\cos(2\theta-2\theta_{\text{refr}}) - R\cos(2\theta-2\theta_{\text{refr}}-(\pi-2\theta_{\text{refr}})))}{1-2R\cos(\pi-2\theta_{\text{refr}})+R^2}\right), \\
&= \frac{n_2 P}{c}\left(1+\cos 2\theta - \frac{T^2(\cos(2\theta-2\theta_{\text{refr}}) - R\cos(2\theta-\pi))}{1-2R\cos(\pi-2\theta_{\text{refr}})+R^2}\right), \\
&= \frac{n_2 P}{c}\left(1+\cos 2\theta - \frac{T^2(\cos(2\theta-2\theta_{\text{refr}}) + R\cos 2\theta)}{1+2R\cos 2\theta_{\text{refr}}+R^2}\right).
\end{aligned}$$

Similarly, applying trigonometric identities,

$$\begin{aligned}
\sum_{n=0}^{\infty} R^n \sin(\alpha+n\beta) &= \sum_{n=0}^{\infty} R^n(\sin\alpha\cos n\beta + \cos\alpha\sin n\beta), \\
&= \sin\alpha\sum_{n=0}^{\infty} R^n\cos n\beta + \cos\alpha\sum_{n=0}^{\infty} R^n\sin n\beta
\end{aligned}$$

Applying Eq. 1.447.1&2 in Ref. [76],

$$\begin{aligned}
\sum_{n=0}^{\infty} R^n \sin(\alpha+n\beta) &= \sin\alpha\times\frac{1-R\cos\beta}{1-2R\cos\beta+R^2} + \cos\alpha\times\frac{R\sin\beta}{1-2R\cos\beta+R^2}, \\
&= \frac{\sin\alpha + R(\cos\alpha\sin\beta - \sin\alpha\cos\beta)}{1-2R\cos\beta+R^2}, \\
&= \frac{\sin\alpha + R\sin(\beta-\alpha)}{1-2R\cos\beta+R^2}. \qquad \text{(A.2)}
\end{aligned}$$

Applying $\sin(\pi + 2\theta) = -\sin 2\theta$ and substituting Eq.$A.2$ into f_{grad}, the gradient force generated by a single ray is expressed as:

$$\begin{aligned}
f_{\text{grad}} &= -\frac{n_2 P}{c}\left(-\sin 2\theta + T^2 \times \frac{\sin\alpha + R\sin(\beta-\alpha)}{1-2R\cos\beta+R^2}\right), \\
&= \frac{n_2 P}{c}\left(\sin 2\theta - \frac{T^2\left(\sin(2\theta-2\theta_{\text{refr}}) + R\sin(\pi-2\theta_{\text{refr}}-(2\theta-2\theta_{\text{refr}}))\right)}{1-2R\cos(\pi-2\theta_{\text{refr}})+R^2}\right), \\
&= \frac{n_2 P}{c}\left(\sin 2\theta - \frac{T^2\left(\sin(2\theta-2\theta_{\text{refr}}) + R\sin(\pi-2\theta)\right)}{1-2R\cos(\pi-2\theta_{\text{refr}})+R^2}\right), \\
&= \frac{n_2 P}{c}\left(\sin 2\theta - \frac{T^2\left(\sin(2\theta-2\theta_{\text{refr}}) + R\sin 2\theta\right)}{1+2R\cos 2\theta_{\text{refr}}+R^2}\right).
\end{aligned}$$

A.2 Calculations in the Steering System

To have a full steering capability, two sets of lenses are recommended. One is used to steer in the transverse direction, and the other is for steering in the axial direction. If the distance between the steering lenses and the objective is chosen properly, this will correspond to a similar deflection before entering the objective lens and a resulting lateral translation in the sample plane. The position of the beam waist, that is the focus of the optical trap, can be adjusted by an axial displacement of the initial lens. Such an axial displacement causes the beam to diverge or converge slightly, the end result of which is an axially displaced position of the beam waist in the sample chamber.[22]

A.2.1 Steering in the Axial Direction

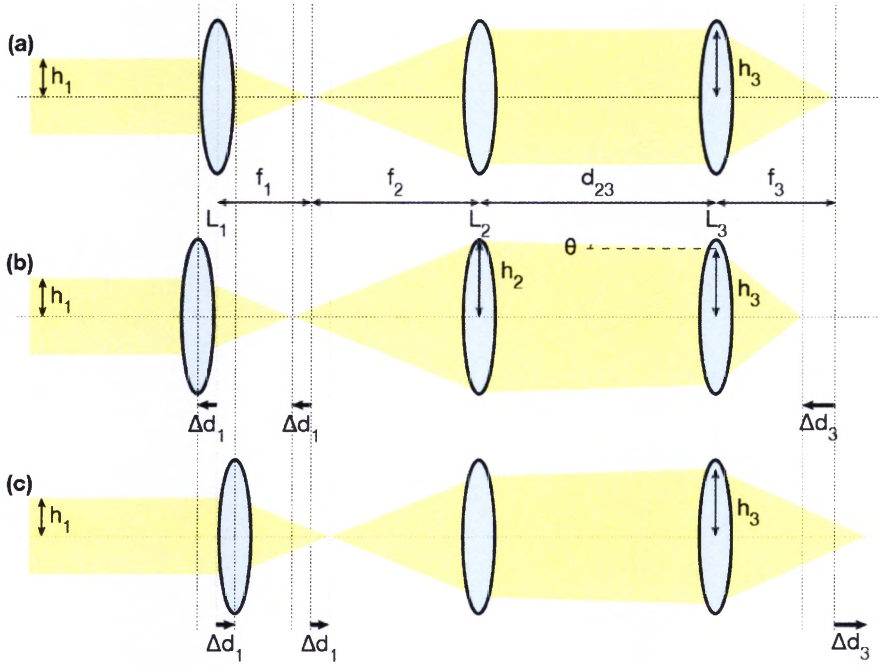

Figure A.1: Schematic of Steering in the Axial Direction.

To calculate the beam radius on the lens L_3 when the lens L_1 is moved along the optical axis with displacement Δd_1. Based on geometrical optics between the lenses L_1 and L_2,

$$\frac{h_1}{f_1} = \frac{-h_2}{d_{12} - f_1},$$

or

$$h_2 = -\frac{d_{12} - f_1}{f_1} h_1,$$

where f_1 and f_2 are the respective focal lengths of the lenses L_1 and L_2, h_1 and h_2 are the respective beam radii on the lenses L_1 and L_2, and d_{12} is the separation distance between the lenses L_1 and L_2. In addition, the tangent of the angle θ in Fig.() is expressed as:

$$\tan\theta = \frac{h_2 - h_3}{d_{23}},$$

where h_3 are the beam radius on the lens L_3, and d_{23} is the separation distance between the lenses L_2 and L_3. From the thin lens equation on the lens L_2,

$$\frac{1}{f_2} = \frac{1}{d_{12} - f_1} + \frac{1}{x},$$

where x is the location of the image and is expressed as:

$$x = \left(\frac{1}{f_2} - \frac{1}{d_{12} - f_1}\right)^{-1}.$$

The angle θ is also expressed as:

$$\tan\theta = \frac{h_2}{x} = h_2\left(\frac{1}{f_2} - \frac{1}{d_{12} - f_1}\right).$$

Hence, we may obtain

$$\frac{h_2 - h_3}{d_{23}} = h_2\left(\frac{1}{f_2} - \frac{1}{d_{12} - f_1}\right),$$

and solve for h_3:

$$\begin{aligned} h_3 &= h_2 - d_{23}h_2\left(\frac{1}{f_2} - \frac{1}{d_{12}-f_1}\right), \\ &= -\frac{d_{12}-f_1}{f_1}h_1 + d_{23}\frac{d_{12}-f_1}{f_1}h_1\left(\frac{1}{f_2} - \frac{1}{d_{12}-f_1}\right), \\ &= -\frac{d_{23}}{f_1}h_1 + \frac{(d_{12}-f_1)(d_{23}-f_2)}{f_1 f_2}h_1. \end{aligned}$$

by substituting h_2. When the distance d_{23} between the lenses L_2 and L_3 fulfills the condition:

$$d_{23} = f_2,$$

the beam radius h_3 on the lens L_3 is independent of any displacement on the lens L_1 and becomes:

$$h_3 = -\frac{f_2}{f_1}h_1.$$

To figure out how the displacement Δd_1 of the lens L_1 affects the focal point of the lens L_3, the thin lens equation on the lens L_2 is also expressed as:

$$\frac{1}{f_2} = \frac{1}{f_2 + \Delta d_1} + \frac{1}{x_{i2}}.$$

Then, the image distance x_{i2} of the lens L_2 is

$$x_{i2} = \frac{(f_2 + \Delta d_1) f_2}{\Delta d_1}.$$

Thus, the object distance x_{o3} for the lens L_3 is

$$x_{o3} = d_{23} - \frac{(f_2 + \Delta d_1) f_2}{\Delta d_1}.$$

Applying the thin lens equation for the lens L_3, we may obtain

$$\frac{1}{f_3} = \frac{1}{f_3 + \Delta d_3} + \frac{1}{x_{o3}},$$

where Δd_3 is the corresponding displacement of the focal point of the lens L_3. Solving for Δd_3, we may obtain

$$\begin{aligned} \frac{\Delta d_3}{f_3 (f_3 + \Delta d_3)} &= \frac{\Delta d_1}{d_{23}\Delta d_1 - \Delta d_1 f_2 - f_2^2}, \\ \Delta d_3 &= -\frac{f_3^2 \Delta d_1}{f_2^2 + f_2 \Delta d_1 + f_3 \Delta d_1 - d_{23}\Delta d_1}, \end{aligned}$$

by substituting x_{o3}. In case of $d_{23} = f_2$, the corresponding displacement Δd_3 of the focal point of the lens L_3 becomes:

$$\Delta d_3 = -\frac{f_3^2 \Delta d_1}{f_2^2 + f_3 \Delta d_1}.$$

Due to Δd_1 is much smaller than f_2 in practice, the corresponding displacement Δd_3 is approximately equal to:

$$\Delta d_3 \approx -\left(\frac{f_3}{f_2}\right)^2 \Delta d_1.$$

A.2.2 Steering in the Transverse Direction

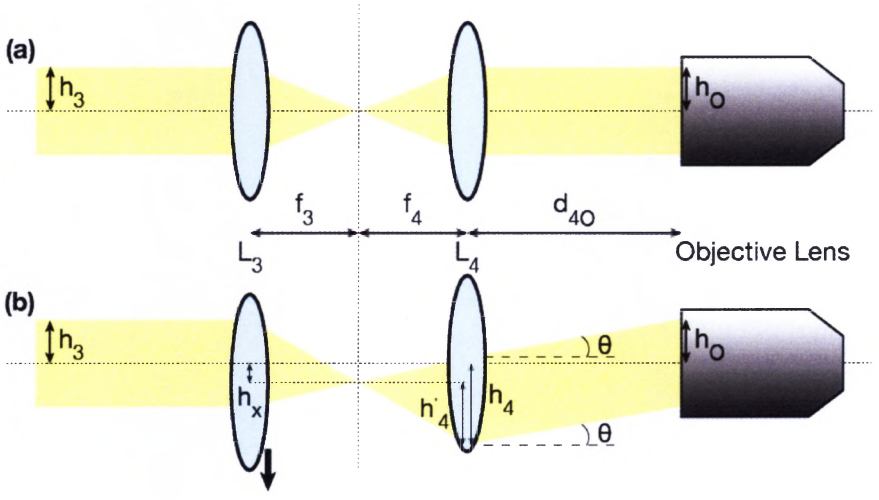

Figure A.2: Schematic of Steering in the Transverse Direction.

In case where the lens L_3 is moved downwards from the optical axis of the objective lens with displacement h_x. Based on geometrical optics, the tangent of the angle θ in Fig.() is

$$\tan\theta = -\frac{h_x}{f_4},$$

where f_4 is the focal length of the lens L_4. In addition, the beam size on the lens L_4 from the center of the lens L_3 (off the optical axis) to the lower boundary of the beam, denoted as h'_4, is expressed as:

$$\frac{h_3 + h_x}{f_3} = \frac{h'_4}{f_4},$$

where h_3 is the beam radius on the lens L_3 and f_3 is the focal length of the lens L_3. Or,

$$h'_4 = -\frac{f_4}{f_3}(h_3 + h_x).$$

Then, the beam size h_4 from the center of lens L_4 (on the optical axis) to the beam lower boundary is

$$\begin{aligned} h_4 &= h'_4 + h_x, \\ &= -\frac{f_4}{f_3}(h_3 + h_x) + h_x. \end{aligned}$$

Hence, the angle θ is also expressed as:

$$\tan\theta = \frac{-\frac{f_4}{f_3}(h_3 + h_x) + h_x - h_O}{d_{4O}},$$

where h_O is the radius of input beam that enters into an objective lens and d_{4O} is the distance between the lens L_4 and the objective lens. Then,

we can obtain

$$-\frac{h_x}{f_4} = -\frac{-\frac{f_4}{f_3}(h_3 + h_x) + h_x - h_O}{d_{4O}},$$

and solve for h_O:

$$\begin{aligned} h_O &= \frac{d_{4O}}{f_4}h_x - \frac{f_4}{f_3}(h_3 + h_x) - h_x, \\ &= -\frac{f_4}{f_3}h_3 + \left(d_{4O} - \frac{(f_3 + f_4)\, f_4}{f_3}\right)\frac{h_x}{f_4}, \end{aligned}$$

Note that the maximum of h_O cannot exceed the half of the entrance pupil diameter of the objective lens. From the expression of h_O, when the distance d_{4O} between the lens L_4 and the objective lens fulfills the condition:

$$d_{4O} = \frac{(f_3 + f_4)\, f_4}{f_3},$$

the radius h_O of input beam that enters into an objective lens is independent of the steering displacement h_x on the lens L_3 and becomes:

$$h_O = -\frac{f_4}{f_3}h_3.$$

To negate any effects of a convergent or divergent beam entering the lens L_3, the lens L_3 must be conjugate to the entrance pupil of the objective lens with the beam size at the lens L_3 remaining the same.

The configuration will not change the beam at the entrance pupil. To figure out how the axial displacement Δd_3 of the lens L_3 affects the effective focal point of the objective lens, the thin lens equation on the lens L_4 is also expressed as:

$$\frac{1}{f_4} = \frac{1}{f_4 + \Delta d_3} + \frac{1}{x_{i4}}.$$

Then, the image distance x_{i4} of the lens L_4 is

$$x_{i4} = \frac{(f_4 + \Delta d_3)\, f_4}{\Delta d_3}.$$

Thus, the object distance x_{oO} for the objective lens is

$$x_{oO} = d_{4O} - \frac{(f_4 + \Delta d_3)\, f_4}{\Delta d_3}.$$

Applying the thin lens equation for the objective lens, we may obtain

$$\frac{1}{f_{EFL}} = \frac{1}{f_{EFL} + \Delta d_{EFL}} + \frac{1}{x_{oO}},$$

where f_{EFL} is the effective focal length (EFL) of the objective lens and Δd_{EFL} is the corresponding displacement of the effective focal point of

the objective lens. Solving for Δd_{EFL}, we may obtain

$$\begin{aligned} \frac{\Delta d_{EFL}}{f_{EFL}\left(f_{EFL}+\Delta d_{EFL}\right)} &= \frac{\Delta d_3}{d_{4O}\Delta d_3 - \Delta d_3 f_4 - f_4^2}, \\ \Delta d_{EFL} &= -\frac{f_{EFL}^2 \Delta d_3}{f_4^2 + f_4\Delta d_3 + f_{EFL}\Delta d_3 - d_{4O}\Delta d_3}, \end{aligned}$$

by substituting x_{oO}. In case of $d_{4O} = f_4$, the corresponding displacement Δd_{EFL} of the effective focal point of the objective lens becomes:

$$\Delta d_{EFL} = -\frac{f_{EFL}^2 \Delta d_3}{f_4^2 + f_{EFL}\Delta d_3}.$$

Due to Δd_3 is much smaller than f_4 in practice, the corresponding displacement Δd_{EFL} is approximately equal to:

$$\Delta d_{EFL} \approx -\left(\frac{f_{EFL}}{f_4}\right)^2 \Delta d_3.$$

Overall, in case where the lens L_1 is moved along the optical axis with displacement Δd_1, the corresponding displacement Δd_{EFL} of the effective focal point of the objective lens is

$$\Delta d_{EFL} \simeq \left(\frac{f_{EFL}}{f_4}\right)^2 \left(\frac{f_3}{f_2}\right)^2 \Delta d_1,$$

which agree with the results in Ref. [77].

A.3 Calculations of Calibration Methods

A.3.1 Power Spectral Density Methods

Note that the properties of thermal force are

$$\langle F(t) \rangle = 0,$$

and

$$\langle F(t) F(t') \rangle = 2\gamma k_B T \delta(t - t'),$$

where $\delta(t - t')$ is a delta function. Then, the Fourier transform of such a force gives a constant power spectral density function, denoted as S_{xx}:

$$S_{xx} = |F(F_{\text{ext}}(t))|^2 = 4\gamma_x k_B T, \tag{A.3}$$

where $F(F_{ext}(t))$ is the Fourier transform of $\overrightarrow{F}_{ext}(t)$. Then, the Fourier transformation of the non-zero terms in Eq.4.1 are

$$\begin{aligned} F\left(\gamma \frac{dx(t)}{dt}\right) &= \gamma F\left(\frac{dx(t)}{dt}\right), \\ &= -i\omega\gamma X(\omega), \end{aligned}$$

and

$$\begin{aligned} F\left(\kappa x\left(t\right)\right) &= \kappa F\left(x\left(t\right)\right), \\ &= \frac{\kappa}{\sqrt{2\pi}}\int_{-\infty}^{\infty} dt x\left(t\right)\exp\left(i\omega t\right), \\ &= \kappa X\left(\omega\right), \end{aligned}$$

respectively, where

$$X\left(\omega\right) \equiv \frac{1}{\sqrt{2\pi}}\int_{-\infty}^{\infty} dt x\left(t\right)\exp\left(i\omega t\right).$$

Note that $\omega = 2\pi f$,

$$\begin{aligned} F\left(\gamma\frac{dx\left(t\right)}{dt}\right) + F\left(\kappa x\left(t\right)\right) &= \left(-i\omega\gamma + \kappa\right)X\left(\omega\right), \\ &= \left(-2i\pi\gamma f + \kappa\right)X\left(f\right), \\ &= 2\pi\gamma\left(-if + f_c\right)X\left(f\right), \end{aligned}$$

by substituting the corner frequency $f_c = \frac{\kappa}{2\pi\gamma}$. As a result, we may obtain

$$2\pi\gamma\left(f_c - if\right)X\left(f\right) = F\left(F_{\text{ext}}\left(t\right)\right).$$

To calculate the power spectral density function S_{xx},

$$4\pi^2\gamma^2\left(f^2 + f_c^2\right)\left|X\left(f\right)\right|^2 = \left|F\left(F_{\text{ext}}\left(t\right)\right)\right|^2 = 4\gamma k_B T.$$

Or,

$$S_{xx}(f) = |X(f)|^2 = \frac{k_B T}{\gamma \pi^2 (f^2 + f_c^2)}.$$

A.3.2 Viscous Drag Force Calibration

Applying a constant velocity with a function in piezostage, the velocity $v(t)$ of the medium is given as:

$$v(t) = v_0 \cos \omega t = \omega x_0 \cos \omega t,$$

where $\omega = \frac{v_0}{x_0}$ is the angular frequency and x_0 is the amplitude. The external force acting on a trapped particle is

$$\overrightarrow{F}_{ext}(t) = \gamma \overrightarrow{v}(t),$$

Eq.4.1 becomes

$$\gamma \frac{dx}{dt} + \kappa x = x_0 \gamma \omega \cos \omega t, \tag{A.4}$$

Eq.A.4 has a general solution:

$$x(t) = x_h(t) + x_p(t),$$

where the homogeneous solution for is

$$x_h(t) = x(0)\exp(-\omega_c t),$$

where $\omega_c = 2\pi f_c \equiv \frac{\kappa}{\gamma}$ is the angular corner frequency. For a particular solution for Eq.$A.4$, we may try

$$x_p(t) = A\sin\omega t + B\cos\omega t. \tag{A.5}$$

where A and B are constants. Then,

$$\frac{dx_p(t)}{dt} = \omega A\cos\omega t - \omega B\sin\omega t. \tag{A.6}$$

Substituting Eqs.$A.5$ and $A.6$ into Eq.$A.4$,

$$\begin{aligned}\gamma(\omega A\cos\omega t - \omega B\sin\omega t) + \kappa(A\sin\omega t + B\cos\omega t) &= x_0\gamma_0\omega\cos\omega t,\\ (\gamma\omega A + \kappa B)\cos\omega t + (\kappa A - \gamma\omega B)\sin\omega t &= x_0\gamma_0\omega\cos\omega t.\end{aligned}$$

Hence,

$$\kappa A - \gamma\omega B = 0,$$

and

$$\gamma\omega A + \kappa B = x_0\gamma_0\omega.$$

Then, A and B are expressed as:

$$A = \frac{x_0 \omega^2}{\omega_c^2 \left(1 + \frac{\omega^2}{\omega_c^2}\right)}, \tag{A.7}$$

and

$$B = \frac{x_0 \omega}{\omega_c \left(1 + \frac{\omega^2}{\omega_c^2}\right)}, \tag{A.8}$$

respectively. In addition, applying trigonometric identities, an alternative expression for Eq.$A.5$ is

$$\begin{aligned} x_p(t) &= C \sin(\omega t + D), \\ &= C \cos D \sin \omega t + C \sin D \cos \omega t, \end{aligned}$$

where C and D are another set of constants. Thus,

$$A = C \cos D,$$

and

$$B = C \sin D.$$

Then, C and D can be expressed in terms of A and B as:

$$C = \sqrt{A^2 + B^2},$$

and

$$D = \arctan \frac{B}{A}.$$

Substituting Eqs.$A.7$ and $A.8$ into C and D,

$$C = \frac{x_0 f}{\sqrt{f^2 + f_c^2}}.$$

and

$$D = \arctan \frac{f_c}{f}$$

in terms of f and f_c. Thus, applying the viscous medium velocity $v(t) = v_0 \cos \omega t$ on the piezostage, the force applied by the laser on the trapped spherical particle is

$$F(t) = -\kappa x(t) = -\frac{\kappa x_0}{\sqrt{1 + \left(\frac{f_c}{f}\right)^2}} \sin\left(2\pi f t + \arctan \frac{f_c}{f}\right).$$

Appendix B

Experimental Procedures

B.1 Optical Trapping

B.1.1 Operation of a Laser

1. Make sure a safety goggle has been worn and all beam paths have been properly blocked. Connect the Ethernet from the M-Squared laser controller to a computer.
2. Turn on the pump laser power source (532 nm) and the M-Squared laser controller.
3. The M-Squared laser requires the output power of the pump source at 15 W. Turn the knob on the pump laser power supply to increase power to 15 W and press the knob to setup the power. Wait the power of the pump source ramping and allow additional 30 min for

the pump source to be stabilized.

4. Open a Google Chrome tab and connects to IP address: 192.168.1.222. That is the IP address of the M-Squared laser controller. Note that a username and a password are required to access the control system.

5. Make sure that the M-Squared laser is lasing properly. Adjust the wavelength on the control web page and follow by an "One Shot"alignment to automatically find the optimal output at the wavelength. Note that 780 nm is the wavelength of the optimal performance of this laser and has the output power about 4 to 5 W. 960 nm is the wavelength for the QPD from Thorlabs Inc. (Model No. $PDQ80A$) with the maximum responsibility for the signal detection, which is the preferable detection wavelength for the QPD.

   - Ideally, after the "One Shot"alignment, neither the $X-$ nor $Y-$axis readings should be extreme.
   - Output voltage displayed on the control web page should be no less than 1 V.
   - Once the wavelength is changed, repeat the "One Shot"alignment.

6. After the completiion of the "One Shot"alignment, apply the Etalon lock on the control web page. Then, visual check the beam profile along its path.

B.1.2 Operation of a Microscope

1. Turn on the microscope power. Make sure that the laser beam path is blocked properly. Adjust the intensity of the illumination source to a comfortable setting. Switch the field of view to the eyepiece.
2. Load a sample slide onto the stage. Select a low magnification objective lens and bring the sample into focus.
    - A simple method for focusing a microscope is to carefully move the specimen close to the objective lens using the coarse focus knob, watching its approach by naked eye. Then, adjust the focus by moving the specimen away from the objective lens.
3. Make sure that the microscope condenser is on the bright-field if it is multi-functional (such as bright-field, dark-field, phase contrast, etc). Close down the field diaphragm which is located on the top near the lamp.
4. Use the condenser focus knob, adjust the image of the field diaphragm until the edges of the diaphragm can be seen via the eyepiece.
    - A simple method for imaging the field diaphragm is to carefully move the condenser close to the sample slide using the condenser focus knob, watching its approach by naked eye. Then,

adjust the image by moving the condenser away from the slide.

5. Use the condenser centering screws to move the image of the field diaphragm into the center of the viewing area visible in the microscope.

6. Open up the field diaphragm so that the edges of the field diaphragm image are just outside the viewing area visible in the microscope. Opening the field diaphragm any farther results in loss of contrast.

7. Adjust the condenser diaphragm by closing it down until the specimen just starts to get dark and no further. While this by eye adjustment is usually satisfactory, a more accurate assessment can be done by removing an eyepiece and checking to see that the condenser diaphragm covers about 75% of the field. The microscope should achieve Köhler illumination at this point. Switch the field of view to a camera and adjust the intensity of the illumination source which gives a good contrast on the image but not over exposed.

8. Repeat steps 3 to 6 if the objective lens is changed.

B.1.3 Optical Tweezers

1. Start aligning Köhler illumination with an oil-immersion objective lens with high NA because optical trapping requires a steep axial gradient. Then, place a dichroic mirror on the top of the condenser.
2. Open the condenser diaphragm which allows forward scattered laser beam from the specimen to pass through and to be detected by a QPD at the BFP of the condenser.
3. Via the software of the CCD camera, visual check the trap profile and attempt to trap a particle.
4. Turn on the QPD power. The QPD mode should not be on closed or open loop settings by holding the "Mode"button for more than 5 s.
5. Unblock the beam path and make sure that the laser beam passing through the condenser projects onto the QPD sensor.
6. Using a LabVIEW program called "Voltage - signal check.vi"to fine adjust the QPD position so that $x-$ & $y-$ signals are close to zero. Note that perform the fine adjustment while a single particle is trapped. In addition, run another LabVIEW program called "OnlineCalibration.vi"to roughly test the trap quality via a quick fitted Lorentzian shape curve.

- The attenuation may be placed in the front of the QPD to prevent over exposure. It depends on the $z-$signal. Ideally, it should be under 5 V on average.

7. Record data with "Voltage - Continuous Input.vi"and save it as ".txt"file.

B.1.4 Shutting Down

- To shut down the laser, close the shutter on the pump source. Turn off the power of the pump source. Turn keys to off position on power supplies of the pump source and the M-Squared laser controller. Block and clear beam paths.
- To shut down the microscope, turn off the power of the microscope and remove any sample slide from the stage. Clean the objective lens and the condenser with a lens tissue paper when immersion materials are applied. Turn off the CCD camera. Cover up the microscope to protect dusts and airborne particles.
- Cover up the optical table to protect dusts and airborne particles.

B.2 Immunocytochemistry Experiment

Immunocytochemistry (ICC) is used to understand the distribution and localization of proteins within compartments of a cell. ICC detects specific antigens in preserved cell populations using an appropriate antibody labeling strategy. Samples are collected, fixed to maintain cell morphology, architecture and the antigenicity of target epitopes. A variety of antibody staining schemes can produce informative ICC images. Having an antibody conjugated to a fluorophore (immunofluorescence) is a common detection method.

B.2.1 Experimental Procedures

It is recommended that the cells are grown on 100 mm or 150 mm diameter tissue culture dishes and that the cells are then seeded on 6−well tissue culture plates before the day of the experiment. Seed adherent cells on 6−well tissue culture plates in a sterile tissue culture hood.

Preparation of the Cells

1. Sterilize glass coverslips by dipping them in 90% *ethanol* and carefully drying them over a flame for a few seconds.
2. Place each coverslip in sterile 6−well tissue culture plates.

3. Add 1 to 2 mL of cell suspension over each coverslip in the 6−well plates.
4. Grow the cells at 37 °C in a humidified incubator for 1 to 2 h.

Fixation of the Cells

1. Aspirate the culture medium from each well and gently rinse the cells twice in *PBS* at room temperature. Do not let the cells dry out.
2. Fix the cells by incubating them in 4% (v/v) *paraformaldehyde* in *PBS* for 20 min at room temperature.
3. Rinse the cells three times with *PBS*.
    - Optional: The cells can be stored in 0.02% (w/v) *sodium azide* in *PBS* at 4 °C for several days.

Permeabilization and Staining

1. Incubate the cells in 0.1% *Triton X-100* in *PBS* for 15 min at room temperature.
2. Rinse the cells 3 times in *PBS*.
3. Incubate the cells in 10% *BSA* in *PBS* for 1 h at room temperature.

4. Dilute the primary monoclonal antibody/antibodies to the appropriate concentration using *block solution*; the final volume should be sufficient to cover each coverslip (1 mL per coverslip).
    - Dye: 1 µL *PI Stock* in 1 mL solution
5. Incubate the cells in the primary antibody/antibodies at 4 °C overnight, or at room temperature for 2 h.
6. Rinse the cells in 1% *BSA* in *PBS* three times for 10 min.
7. Rinse cells away from light in 1% *block solution* three times for 10 min.
8. Label a microscope slide for each coverslip.
9. Add a drop of *mounting medium* to each slide.
10. Pick up each coverslip with a forceps and place it on the *mounting medium*, with the cell-side face down.
11. Apply nail polish or glue along the edges of the coverslips to seal them to the slides.
12. Visualize the cells using a fluorescence microscope equipped with the appropriate filters for *PI* dye.

B.2.2 Materials Needed

- 4% (v/v) *paraformaldehyde*

  - 10 mL 40% *paraformaldehyde*
  - 90 mL 1*X PBS*

- 1 L 10*X PBS* at *pH* 7.2 to 7.4
  - 10.9 g *Disodium Phosphate*
  - 3.2 g *Monosodium Phosphate*
  - 90 g *Sodium Chloride*
  - Balance *pH* with *Hydrochloric Acid* and *Sodium Hydroxide Solution*, then bring the final volume up to 1 L

- *Propine Iodide (PI) Stock*
  - 1 µg *Propine Iodide* dissolves in 1 mL water

- 1% *Bovine Serum Albumin* (*BSA*)
  - 1 µg *BSA* dissolves in 100 mL water

- *Block Solution*
  - 1% *PBS*
  - 0.1% Cold Fish Skin Gelatin
  - 0.5% *Triton X-100*
  - 0.05% *Sodium Azide*
  - 0.01 mol L^{-1} *PBS* at *pH* 7.2 to 7.4
  - 1% *PBS*

- *Mounting Medium*
  - 1 part of $10X$ *PBS*
  - 9 part of *Glycerol* (ACS grade 99% to 100% purity)
  - 0.1 part of 20% *n-propyl gallate* dropwise with rapid stirring
    * Note that *n-propyl gallate* does not dissolve well in water-based solutions. Instead, use *dimethyl formamide* or *dimethyl sulfoxide* as a solvent.
- 6−well tissue culture plate

B.2.3 Instruments

- Fluorescence Microscope
- Sterile tissue culture hood
- 37 °C incubator

B.3 Colony-Forming Unit Experiment

We plan to perform colony-forming unit (CFU) for *E. coli* $MG1655$ ($JOE4212$) grown in LB and TY before and after laser treatment (532 nm for damage and 1064 nm for positive control). Each time, we propose to

perform CFU only for one bacterial strain which is grown in one medium and repeat three times. The experiment usually takes two days.

B.3.1 Experimental Procedures

The night before CFU and Laser treatment, grow overnight cultures for a bacterial strain in *LB* or *TY* medium.

Day ONE

1. Obtain overnight cultures. Turn on spectrometer to measure $OD_{600\,\mathrm{nm}}$. Calculate the concentration of culture stock. Then, dilute the overnight culture with sterile growth medium to obtain $OD_{600\,\mathrm{nm}} = 0.1$ suspension before Laser treatment. Dilute to 6 mL and use 1 mL to check $OD_{600\,\mathrm{nm}}$.
2. Take the suspension to Thornton Hall 212. Carefully check laser alignments before the treatment. Use 35 mm in diameter petri dishes, which can hold at least 1 mL of liquid, or alternative chambers for exposure.
3. Make three aliquots of the suspension. One is a negative control which will sit on the side at the room temperature. One is a positive control which will be treated under 1064 nm at the room temperature. And one is a damage experiment which will be treated under

532 nm at the room temperature.

4. Fill up the chamber and place the chamber in the laser pathway. Turn on the lasers and let them stay at max power output. Start the treatments by 532 nm and 1064 nm simultaneously for one to two hours [exposure time will have to be determined empirically; should be similar to timing of laser treatment in optical traps]. There are two options for laser treatments:
   (a) The laser beam is broad which could cover up the full size of the chamber. The power density may be too low. We need to test on that. [This is preferable.]
   (b) The laser beam is focused inside the chamber and the treating area is relatively small. Mix the suspension by a pipette every ten to fifteen minutes. [This is difficult to ensure that all cells are treated for equal amounts of time.]
5. After treatments, recover the treated samples as much as possible and take them back to Hensil Hall 624.
6. Measure $OD_{600\,\mathrm{nm}}$ of the negative control to calculate the bacterial concentration. Assume that bacterial concentrations are the same in controls and Laser treatment. [This step may not be necessary, since appropriate controls have been included.]
7. Start to perform serial dilutions for all three suspensions. The serial

dilution factor is $\frac{1}{10}$. Plate 100 µL of 10^{-4}, 10^{-5} and 10^{-6} dilutions separately on three agar plates for each suspension. This needs to be done in replicates for each sample. For one bacterial species in one medium, six are for negative controls, six are for positive controls (1064 nm), and six are for laser treatment at 532 nm. In total, 18 plates are required each time.

8. Incubate the plates overnight at 37 °C.

Day TWO

- Count colonies, possibly also noting if colony sizes vary in different samples.
- Calculation of total colony forming units in CFU per mL:

$$\text{CFU per mL} = \frac{\text{No. of Colonies} \times \text{Dilution Factor}}{\text{Volume of Plating Culture}}$$

- Comparison of CFU per mL of negative and positive controls and treatment with 532 nm laser.

B.3.2 Materials Needed

- Sterile *TY* media
- Sterile *LB* media

- Sterile water for serial dilutions
- *TY* Agar plates (18 for each trial)
- *LB* Agar plates (18 for each trial)
- Three trials after initial determination of optimal conditions (such as exposure duration)
- 35 mm petri dishes for laser exposure
- 48−well or 24−well plates for serial dilutions

B.3.3 Instruments

- Spectrophotometer and cuvettes for OD measurements
- 532 nm Laser
- 1064 nm Laser
- 37 °C incubator

Bibliography

[1] Arthur Ashkin, Joseph M. Dziedzic, J. E. Bjorkholm, and Steven Chu. Observation of a single-beam gradient force optical trap for dielectric particles. *Optics Letters*, 11(5):288–90, May 1986.

[2] Arthur Ashkin. Forces of a single-beam gradient laser trap on a dielectric sphere in the ray optics regime. *Biophysical Journal*, 61(2):569–82, February 1992.

[3] Arthur Ashkin. Acceleration and trapping of particles by radiation pressure. *Physical Review Letters*, 24(4):156–9, January 1970.

[4] Michael P. MacDonald, Gabriel C. Spalding, and Kishan Dholakia. Microfluidic sorting in an optical lattice. *Nature*, 426(6965):421–4, November 2003.

[5] Feng Qian, Sergey Ermilov, David Murdock, William E. Brownell, and Bahman Anvari. Combining optical tweezers and patch clamp for studies of cell membrane electromechanics. *Review of Scientific Instruments*, 75(9):2937–42, September 2004.

[6] Angelo Pommella, Valentina Preziosi, Sergio Caserta, Jonathan M. Cooper, Stefano Guido, and Manlio Tassieri. Using optical tweezers for the characterization of polyelectrolyte solutions with very low viscoelasticity. *Langmuir*, 29(29):9224–30, June 2013.

[7] Steven M. Block, Lawrence S. B. Goldstein, and Bruce J. Schnapp. Bead movement by single kinesin molecules studied with optical tweezers. *Nature*, 348(6299):348–52, November 1990.

[8] Karel Svoboda and Steven M. Block. Biological application of opti-

cal forces. *Annual Review of Biophysics and Biomolecular Structure*, 23:247–85, June 1994.

[9] Jennifer E. Curtis and David G. Grier. Structure of optical vortices. *Physical Review Letters*, 90(13):133901, April 2003.

[10] Miles Padgett and Les Allen. Optical tweezers and spanners. *Physics World*, 10(9):35–8, 1997.

[11] David McGloin and Kishan Dholakia. Bessel beams: diffraction in a new light. *Contemporary Physics*, 46(1):15–28, November 2010.

[12] Keir C. Neuman and Steven M. Block. Optical trapping. *Review of Scientific Instruments*, 75(9):2787–809, September 2004.

[13] Wilfried Grange, Sudhir Husale, Hans-Joachim Guntherodt, , and Martin Hegner. Optical tweezers system measuring the change in light momentum flux. *Review of Scientific Instruments*, 73(6):2308–16, June 2002.

[14] Keir C.Neuman, Edmund H.Chadd, Grace F.Liou, Keren Bergman, and Steven M.Block. Characterization of photodamage to escherichia coli in optical traps. *Biophysical Journal*, 77(5):2856–63, November 1999.

[15] S. Inoue and K. R. Spring. *Video Microscopy*. Plenum Press, New York, 2nd edition, 1997.

[16] Hiroaki Misawa, Masanori Koshioka, Keiji Sasaki, Noboru Kitamura, and Hiroshi Masuhara. Three-dimensional optical trapping and laser ablation of a single polymer latex particle in water. *Journal of Applied Physics*, 70(7):3829, October 1991.

[17] Koen Visscher and Steven M. Block. Versatile optical traps with feedback control. *Methods in Enzymology*, 298(38):460–89, 1998.

[18] Koen Visscher, Mark J. Schnitzer, and Steven M. Block. Single kinesin molecules studied with a molecular force clamp. *Nature*, 400(6740):184–9, July 1999.

[19] Koen Visscher, Steven P. Gross, and Steven M. Block. Construction of multiple-beam optical traps with nanometer-resolution position sensing. *IEEE Journal of Selected Topics in Quantum Electronics*, 2(4):1066–76, December 1996.

[20] Maarten C. Noom, Bram van den Broek, Joost van Mameren, and Gijs J. L. Wuite. Visualizing single dna-bound proteins using dna as a scanning probe. *Nature Methods*, 4(12):1031–6, November 2007.

[21] Jose A. Rodrigo and Tatiana Alieva. Freestyle 3d laser traps: tools for studying light-driven particle dynamics and beyond. *Optica*, 2(9):812, 2015.

[22] D. Bowman, T. L. Harte, V. Chardonnet, C. De Groot, S. J. Denny, G. Le Goc, M. Anderson, P. Ireland, D. Cassettari, and G. D. Bruce. High-fidelity phase and amplitude control of phase-only computer generated holograms using conjugate gradient minimisation. *Optics Express*, 25(10):11692–700, 2017.

[23] Michelle D.Wang, H.Yin, R. Landick, J.Gelles, and Steven M. Block. Stretching dna with optical tweezers. *Biophysical Journal*, 72(3):1335–46, March 1997.

[24] Thomas T. Perkins, Ravindra V. Dalal, Paul G. Mitsis, and Steven M. Block. Sequence-dependent pausing of single lambda exonuclease molecules. *Science*, 301(5641):1914–8, September 2003.

[25] Steven J. Koch and Michelle D. Wang. Dynamic force spectroscopy of protein-dna interactions by unzipping dna. *Physical Review Letters*, 91(2):028103, July 2003.

[26] Brent D. Brower-Toland, Corey L. Smith, Richard C. Yeh, John T. Lis, Craig L. Peterson, and Michelle D. Wang. Mechanical disruption of individual nucleosomes reveals a reversible multistage release of dna. *Proceeding the National Academy of Sciences of the United States of America*, 99(4):1960–5, February 2002.

[27] Steven J. Koch, Alla Shundrovsky, Benjamin C. Jantzen, and Michelle D.Wang. Probing protein-dna interactions by unzipping a single dna double helix. *Biophysical Journal*, 83(2):1098–105, August 2002.

[28] Matthew J. Lang, Charles L. Asbury, Joshua W. Shaevitz, and Steven M. Block. An automated two-dimensional optical force clamp for single molecule studies. *Biophysical Journal*, 83(1):491–501, July 2002.

[29] Astrid van der Horst and Nancy R. Forde. Power spectral analysis for optical trap stiffness calibration from high-speed camera position detection with limited bandwidth. *Optics Express*, 18(8):7670–7, 2010.

[30] Kevin D. Whitley, Matthew J. Comstock, and Yann R. Chemla. High-resolution "fleezers": Dual-trap optical tweezers combined with single-molecule fluorescence detection. *Methods in Molecular Biology*, 1486:183–256, November 2016.

[31] Jeffrey R. Moffitt, Yann R. Chemla, David Izhaky, and Carlos Bustamante. Differential detection of dual traps improves the spatial resolution of optical tweezers. *Proceeding the National Academy of Sciences of the United States of America*, 103(24):9006–11, June 2006.

[32] Bharat Jagannathan and Susan Marqusee. Protein folding and unfolding under force. *Biopolymers*, 99(11):860–9, August 2013.

[33] Jermey N. A. Matthews. Commercial optical traps emerge from biophysics labs. *Physics Today*, 62(2):26–8, February 2009.

[34] Robert W. Applegate, Jeff Squier, Tor Vestad, John Oakey, and David W. M. Marr. Optical trapping, manipulation, and sorting of cells and colloids in microfluidic systems with diode laser bars. *Optics Express*, 12(19):4390–8, 2004.

[35] Optical trapping lab - grup de biofotnica.

[36] Yi Deng, John Bechhoefer, and Nancy R. Forde. Brownian motion in a modulated optical trap. *Journal of Optics A: Pure and Applied Optics*, 9(8):S256, July 2007.

[37] Akbar Samadi, Chensong Zhang, Joseph Chen, S. Nader S. Reihani, and Zhigang Chen. Evaluating the toxic effect of an antimicrobial agent on single bacterial cells with optical tweezers. *Biomedical Optics Express*, 6(1):112–7, January 2015.

[38] Zdenek Pilat, Jan Jezek, M. Sery, Martin Trtilek, Ladislav Nedbal, and Pavel Zemanek. Optical trapping of microalgae at 735-1064 nm: Photodamage assessment. *Journal of Photochemistry and Photobiology B: Biology*, 121:27–31, April 2013.

[39] Erwin J. G. Peterman, Frederick Gittes, and Christoph F. Schmidt. Laser-induced heating in optical traps. *Biophysical Journal*, 84(2):1308–16, February 2003.

[40] Akbar Samadi and Nader S. Reihani. Optimal beam diameter for optical tweezers. *Optics Letters*, 35(10):1494–6, May 2010.

[41] Jean Carlet, Vincent Jarlier, Stephan Harbarth, Andreas Voss, Herman Goossens, Didier Pittet, and the Participants of the 3rd World Healthcare-Associated Infections Forum. Ready for a world without antibiotics? the pensieres antibiotic resistance call to action. *Antimicrobial Resistance and Infection Control*, 1(1):1–11, February 2012.

[42] Karthikeyan K. Kumarasamy, Mark A. Toleman, Timothy R. Walsh, Jay Bagaria, Fafhana Butt, Ravikumar Balakrishnan, Uma Chaudhary, Michel Doumith, Christian G. Giske, Seema Irfan, Padma Krishnan, Anil V. Kumar, Sunil Maharjan, Shazad Mushtaq, Tabassum Noorie, David L. Paterson, Andrew Pearson, Claire Perry, Rachel Pike, Bhargavi Rao, Ujjwayini Ray, Jayanta B. Sarma, Madhu Sharma, Elizabeth Sheridan, Mandayam A. Thirunarayan, Jane Turton, Supriya Upadhyay, Marina Warner, William Welfare, David M. Livermore, and Neil Woodford. Emergence of a new antibiotic resistance mechanism in india, pakistan, and the uk: a molecular, biological, and epidemiological study. *The Lancet Infectious Diseases*, 10(9):597–602, September 2010.

[43] L. Barth Reller, Melvin Weinstein, James H. Jorgensen, and Mary Jane Ferraro. Antimicrobial susceptibility testing: a review of general principles and contemporary practices. *Clinical Infectious Diseases*, 49(11):1749–55, December 2009.

[44] Jacquie T. Keer and L. Birch. Molecular methods for the assessment of bacterial viability. *Journal of Microbiological Methods*, 53(2):175–83, May 2003.

[45] Byron F. Brehm-Stecher and Eric A. Johnson. Single-cell microbiology: tools, technologies, and applications. *Microbiology and Molecular Biology Reviews*, 68(3):538–59, September 2004.

[46] Alex van Belkum and W. Michael Dunne Jr. Next-generation antimicrobial susceptibility testing. *Journal of Clinical Microbiology*, 51(7):2018–24, July 2013.

[47] Arthur Ashkin, Joseph M. Dziedzic, and T. Yamane. Optical trapping and manipulation of single cells using infrared laser beams. *Nature*, 330(6150):769–71, December 1987.

[48] Arthur Ashkin and Joseph M. Dziedzic. Optical trapping and manipulation of viruses and bacteria. *Science*, 235(4795):1517–20, May 1987.

[49] David G. Grier. A revolution in optical manipulation. *Nature*, 424(6950):810–6, August 2003.

[50] David McGloin and J. P. Reid. Forty years of optical manipulation. *Optics and Photonics News*, 21(3):20–6, 2010.

[51] Aline Pellizzaro, Gabriel Welker, David Scott, Rance Solomon, James Cooper, Anthony Farone, Mary Farone, Robert S. Mushi, Maria del Pilar Aguinaga, and Daniel Erenso. Direct laser trapping for measuring the behavior of transfused erythrocytes in a sickle cell anemia patient. *Biomedical Optics Express*, 3(9):2190–9, September 2012.

[52] Guan-Bo Liao, Yin-Quan Chen, Paul B. Bareil, Yunlong Sheng, Arthur Chiou, and Ming-Shien Chang. Radiation pressure on a biconcave human red blood cell and the resulting deformation in a pair of parallel optical traps. *Journal of Biophotonics*, 7(10):782–7, October 2014.

[53] Steven M. Block, David F. Blair, and Howard C. Berg. Compliance of bacterial flagella measured with optical tweezers. *Nature*, 338(6215):514–8, April 1989.

[54] Richard M. Berry and Howard C. Berg. Absence of a barrier to backwards rotation of the bacterial flagellar motor demonstrated with optical tweezers. *Proceeding the National Academy of Sciences of the United States of America*, 94(26):14433–7, December 1997.

[55] Taejin L. Min, Patrick J. Mears, Lon M. Chubiz, Christopher V. Rao, Ido Golding, and Yann R. Chemla. High-resolution, long-term

characterization of bacterial motility using optical tweezers. *Nature Methods*, 6(11):831–5, October 2009.

[56] Tuba Altindal, Suddhashil Chattopadhyay, and Xiao-Lun Wu. Bacterial chemotaxis in an optical trap. *PLoS ONE*, 6(4):e18231, April 2011.

[57] Ignacio A. Martnez, Susana Campoy, Meritxell Tort, Montserrat Llagostera, and Dmitri Petrov. A simple technique based on a single optical trap for the determination of bacterial swimming pattern. *PLoS ONE*, 8(4):e61630, April 2013.

[58] M. Ericsson, D. Hanstorp, P. Hagberg, J. Enger, and T. Nystrom. Sorting out bacterial viability with optical tweezers. *Journal of Bacteriology*, 182(19):5551–5, October 2000.

[59] Frederick Gittes and Christoph F. Schmidt. Interference model for back-focal-plane displacement detection in optical tweezers. *Optics Letters*, 23(1):7–9, January 1998.

[60] Akbar Samadi and S. Nader S. Reihani. Role of condenser iris in optical tweezer detection system. *Optics Letters*, 36(20):4056–8, October 2011.

[61] Harry E. Morton. The relationship of concentration and germicidal efficiency of ethyl alcohol. *Annals of the New York Academy of Sciences*, 53(1):191–6, August 1950.

[62] Akira Koshiro and Shigeharu Oie. Bactericidal activity of ethanol against glucose nonfermentative gram-negative bacilli. *Microbios*, 40(159):33–40, February 1984.

[63] Lin Ling, Fei Zhou, Lu Huang, and Zhi-Yuan Li. Optical forces on arbitrary shaped particles in optical tweezers. *Journal of Applied Physics*, 108(7):073110, October 2010.

[64] David B. Phillips, Miles J. Padgett, Simon Hanna, Ying-Lung D. Ho, D. M. Carberry, Mervyn J. Miles, and Stephen H. Simpson. Shape-induced force fields in optical trapping. *Nature Photonics*, 8(5):400–5, April 2014.

[65] Yona Tadir, William H. Wright, Omid Vafa, Teri Ord, Ricardo H. Asch, and Michael W. Berns. Micromanipulation of sperm by a

laser generated optical trap. *Fertility and sterility*, 52(5):870–3, November 1989.

[66] Tudor N. Buican, Miriam J. Smyth, Harry A. Crissman, Gary C. Salzman, Carleton C. Stewart, and John C. Martin. Automated single-cell manipulation and sorting by light trapping. *Applied Optics*, 26(24):5311–6, December 1987.

[67] Arthur Ashkin, Karin Schtze, J. M. Dziedzic, Ursula Euteneuer, and Manfred Schliwa. Force generation of organelle transport measured in vivo by an infrared laser trap. *Nature*, 348(6299):346–8, November 1990.

[68] Steven M. Block. Construction of optical tweezers. In David L. Spector, Robert D. Goldman, and Leslie A. Leinward, editors, *Cells: A Laboratory Manual*, volume 2, chapter 7. Cold Spring Harbor Laboratory Press, Cold Spring Harbor, NY, 1998.

[69] Wei Cheng, Ximiao Hou, and Fangmao Ye. Use of tapered amplifier diode laser for biological-friendly high-resolution optical trapping. *Optical Letters*, 35(17):2988–90, September 2010.

[70] Hans-Peter Grossart, Grieg F. Steward, Josefina Martinez, and Farooq Azam. A simple, rapid method for demonstrating bacterial flagella. *Applied and Environmental Microbiology*, 66(8):3632–6, August 2000.

[71] Howard C. Berg and Robert A. Anderson. Bacteria swim by rotating their flagellar filaments. *Nature*, 245(5425):380–2, October 1973.

[72] Steven M. Block and Howard C. Berg. Successive incorporation of force-generating units in the bacterial rotary motor. *Nature*, 309(5967):470–2, May 1984.

[73] Peter J. Pauzauskie, Aleksandra Radenovic, Eliane Trepagnier, Hari Shroff, Peidong Yang, and Jan Liphardt. Optical trapping and integration of semiconductor nanowire assemblies in water. *Nature Materials*, 5(2):97–101, January 2006.

[74] M. G. Donato, R. Sayed S. Vasi, P. H. Jones, F. Bonaccorso, A. C. Ferrari, P. G. Gucciardi, and O. M. Marag. Optical trapping of nan-

otubes with cylindrical vector beams. *Optics Letters*, 37(16):3381–3, August 2012.

[75] Yasuhiro Harada and Toshimitsu Asakura. Radiation forces on a dielectric sphere in the rayleigh scattering regime. *Optics Communications*, 124(5-6):529–41, March 1996.

[76] Izrail Solomonovich Gradshteyn and Iosif Moiseevich Ryzhik. *Tables of Integrals, Series, and Products.* Academic Press, Oxford, UK, 7th edition, 2007.

[77] Erik Fallman and Ove Axner. Design for fully steerable dual-trap optical tweezers. *Applied Optics*, 36(10):2107–13, April 1997.